

See discussions, stats, and author profiles for this publication at: <https://www.researchgate.net/publication/278396287>

# Charge Transfer Dynamics in Donor–Acceptor Complexes between a Conjugated Polymer and Fluorene Acceptors

ARTICLE *in* THE JOURNAL OF PHYSICAL CHEMISTRY C · DECEMBER 2014

Impact Factor: 4.77 · DOI: 10.1021/jp510543c

---

READS

46

## 8 AUTHORS, INCLUDING:



Olga Parashchuk

Lomonosov Moscow State University

14 PUBLICATIONS 74 CITATIONS

[SEE PROFILE](#)



Igor F Perepichka

Bangor University

125 PUBLICATIONS 3,148 CITATIONS

[SEE PROFILE](#)



Dmitry Paraschuk

Lomonosov Moscow State University

71 PUBLICATIONS 582 CITATIONS

[SEE PROFILE](#)

# Charge Transfer Dynamics in Donor–Acceptor Complexes between a Conjugated Polymer and Fluorene Acceptors

Vlad G. Pavelyev,<sup>†</sup> Olga D. Parashchuk,<sup>‡</sup> Michal Krompiec,<sup>§,⊥</sup> Tatyana V. Orekhova,<sup>||</sup> Igor F. Perepichka,<sup>\*,§</sup> Paul H. M. van Loosdrecht,<sup>†,#</sup> Dmitry Yu. Paraschuk,<sup>‡</sup> and Maxim S. Pshenichnikov<sup>\*,†</sup>

<sup>†</sup>Zernike Institute for Advanced Materials, University of Groningen, Nijenborgh 4, 9747 AG Groningen, The Netherlands

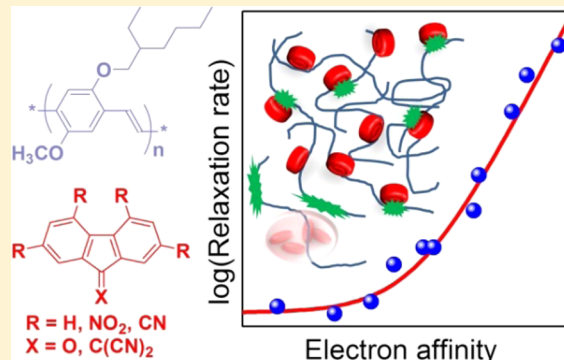
<sup>‡</sup>Faculty of Physics and International Laser Center, Lomonosov Moscow State University, Leninskie Gory, 119991 Moscow, Russia

<sup>§</sup>School of Chemistry, Bangor University, Deiniol Road, Bangor LL57 2UW, United Kingdom

<sup>||</sup>L. M. Litvinenko Institute of Physical Organic and Coal Chemistry, National Academy of Sciences of Ukraine, R. Luxemburg Street 70, Donetsk 83114, Ukraine

## Supporting Information

**ABSTRACT:** We report on ground and excited state charge transfer in charge-transfer complexes in films formed between a semiconducting polymer, MEH-PPV (poly[2-methoxy-5-(2'-ethylhexyloxy)-1,4-phenylenevinylene]), and a series of fluorene electron acceptors. The latter were designed to vary systematically the electron affinity (EA) over  $\sim 1.5$  eV by attachment of various electron withdrawing groups to the fluorene core. The EAs of the acceptors are determined by cyclic voltammetry and compared with those from density functional theory calculations. The charge-transfer dynamics are studied using an ultrafast visible-pump–IR-probe photoinduced absorption technique. We demonstrate that the acceptor EA is the key—but not the only—parameter that governs charge recombination rates that scale exponentially with the acceptor EA. From the time-resolved data we deduced a model that describes charge dynamics for acceptors with low and high EAs. The two opposite trends—higher acceptor EA increases the driving force for charge separation but also inevitably increases the rate of undesirable charge recombination—should be carefully counterbalanced in designing novel polymer–fullerene bulk heterojunctions.



## 1. INTRODUCTION

The electronic ground state of a molecular charge-transfer complex (CTC) is formed by the transfer of a fraction of the electron charge between the noncovalently bound molecular entities, the donor and the acceptor. CTCs and the very process of electron transfer lay at the heart of many photoinduced processes in physics, chemistry, and biology. According to the Mulliken model,<sup>1,2</sup> the amount of the donor–acceptor charge transfer in the CTC ground state is mainly controlled by the difference between the donor ionization potential and the acceptor electron affinity (EA) or in first approximation by the energy difference between the acceptor lowest unoccupied molecular orbital (LUMO) and the donor highest occupied molecular orbital (HOMO), also known as the effective HOMO–LUMO gap.<sup>3</sup>

Upon optical excitation of the Mulliken-type CTCs, a major part of the electron density is transferred from the donor to the acceptor almost instantaneously while the back electron transfer, i.e., charge recombination, occurs within a finite time span.<sup>4,5</sup> The early studies on dynamics of small-molecule CTCs in solutions<sup>6,7</sup> demonstrated that the driving force for geminate

charge recombination is mainly determined by the acceptor EA. The charge recombination rate was shown to scale exponentially with the acceptor EA, while some deviations were attributed to the reorganization energy variations.<sup>6</sup>

In recent years, a new kind of Mulliken-type CTCs involving conjugated polymers as donors has been identified in a variety of polymer–acceptor blends.<sup>8–12</sup> A number of unusual properties makes the polymer-based CTCs especially fascinating in comparison to their small-molecule counterparts. Planarization of the polymer chains<sup>13</sup> and formation of crystalline domains<sup>14</sup> are but two examples. Such properties are closely related to charge delocalization over conjugated polymer chains (nonexisting in small-molecule CTCs) so that the electron density from several repeating units of the polymer is transferred to an acceptor molecule.<sup>13,15</sup>

Ground-state CTCs have also been observed in conjugated polymer–fullerene blends<sup>16</sup> although their absorption is

Received: October 20, 2014

Revised: November 19, 2014

Published: November 19, 2014

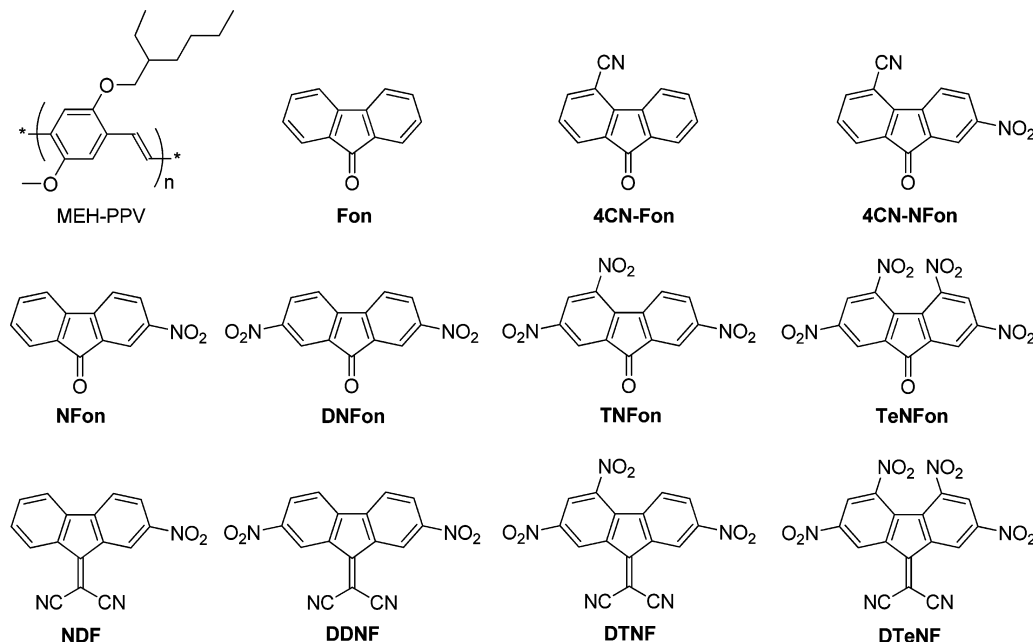


**Figure 1.** Structures of MEH-PPV (upper left) and the studied series of fluorene electron acceptors. Abbreviations of the latter are shown below the structures.

extremely weak,<sup>17–19</sup> partially because CTCs are formed only near the donor–acceptor interface whose volume share is small. In contrast, in polymer–acceptor blends with pronounced ground-state charge transfer, a CTC is formed almost per each conjugated segment so that exciton diffusion and other concurrent processes (e.g., generation of triplets) do not affect the photophysics. As a result, optical excitation leads to immediate formation of a charge-separated state whose charge relaxation dynamics can be readily monitored.<sup>20,21</sup> Furthermore, the new generation of low band gap conjugated polymers for organic photovoltaics (OPV), which have already demonstrated the highest efficiencies in polymer solar cells,<sup>22,23</sup> is built upon a push–pull donor–acceptor concept<sup>24</sup> which extends the light absorption into the red region of the solar spectrum. This is highly reminiscent of Mulliken-type CTC absorption, the difference in the charge-transfer state origin (i.e., covalently linked alternating electron donating and electron accepting monomer units in the polymer backbone vs noncovalently bonded polymer and small-molecule acceptor) notwithstanding.

So far the effect of an acceptor EA on the charge recombination dynamics in conjugated polymer CTCs has only been studied for two commercially available acceptors of different molecular structures.<sup>20,21</sup> As a result, no functional dependences of the charge recombination rates as a function of acceptor EA could have emerged, in sharp contrast to the case of small-molecule CTCs in solutions.<sup>4–7</sup> This calls for a systematic study of charge recombination dynamics in conjugated polymer based CTCs where the acceptor EAs are varied in a controlled and predictable way with as small as possible alternations of the acceptor molecular structure.

In this paper, we report on how the acceptor EA controls the charge recombination dynamics in CTCs between an archetypical conjugated polymer donor, MEH-PPV [poly[2-methoxy-5-(2'-ethylhexyloxy)-1,4-phenylenevinylene]],<sup>25</sup> and a family of small molecular acceptors (Figure 1). A series of fluorene acceptors with a range of EAs was designed, synthesized, and characterized by cyclic voltammetry and

density functional theory (DFT) calculations. The CTC excited state dynamics were studied via generation and recombination of photoinduced charges employing ultrafast visible-pump–IR-probe photoinduced absorption spectroscopy. We show that the recombination rate scales exponentially with the acceptor EA, similar to the earlier observations for small-molecule CTCs in solution.<sup>6,26</sup> Finally, the anisotropy dynamics suggest that separated charges in most of the blends remain highly spatially localized, in sharp contrast to the case of the pristine polymer.

## 2. EXPERIMENTAL SECTION

**2.1. Samples.** Fluorenone (Fon) and 2,7-dinitrofluorenone (DNFon) have been purchased from Sigma-Aldrich and used without further purification. Details of the synthesis of the fluorene acceptors 2-nitrofluorenone (NFon), 2,4,7-trinitrofluorenone (TNFon), 2,4,5,7-tetrinitrofluorenone (TeNFon), 2-nitro-9-dicyanomethylenefluorene (NDF), 2,7-dinitro-9-dicyanomethylenefluorene (DDNF), 2,4,7-trinitro-9-dicyanomethylenefluorene (DTNF), 2,4,5,7-tetrinitro-9-dicyanomethylenefluorene (DTefN), 4-cyanofluorenone (4CN-Fon), and 2-nitro-5-cyanofluorenone (4CN-NFon) and their characterizations are given in the Supporting Information (see the “Synthesis of fluorene acceptors” section and Figures S1–S16 for NMR spectra). Absorption spectra of the acceptors in chlorobenzene (Supporting Information, Figure S17) are situated in the blue-UV region below 450 nm; no signs of aggregation at concentrations up to 2 g·L<sup>−1</sup> were found.

MEH-PPV was chosen as a donor since it is known to readily form a ground-state CTC with fluorene electron acceptors.<sup>12,27</sup> MEH-PPV (Sigma-Aldrich,  $M_n = 86\,000$ ,  $M_w = 420\,000$ ) and fluorene acceptors were dissolved separately in chlorobenzene at a concentration of 2 g·L<sup>−1</sup>. The solutions were placed into an ultrasonic bath for 15 min at 22 °C and then stirred with a magnetic stirrer for ~6 h at 50 °C. Their blends were prepared by mixing the solutions of MEH-PPV and an acceptor with a molar ratio of 1:0.3 per monomer repeat unit. Further increase

of the acceptor concentration in the blends led to phase segregation with loss of sample optical quality.<sup>28</sup>

Films were prepared by drop-casting of MEH-PPV/acceptor solution onto a 150  $\mu\text{m}$  thick microscope cover slide with subsequent drying for 8 h in an air atmosphere at 22 °C. The resulted optical density of the samples did not exceed  $\sim 1.5$  at their maxima. The solution of MEH-PPV with the highest EA acceptor, DTeNF, exhibited strong phase segregation and CTC precipitation, and therefore was not used in the optical experiments. All experiments were performed at ambient conditions; no sample degradation was observed during the experiments.

**2.2. Cyclic Voltammetry.** Electrochemical experiments were carried out using an Autolab PGSTAT-302N potentiostat–galvanostat. Cyclic voltammetry (CV) measurements were performed in a three-electrode cell equipped with a platinum disk ( $d = 1.6$  mm) as the working electrode, platinum wire as a counter electrode, and a nonaqueous Ag/Ag<sup>+</sup> reference electrode (0.01 M AgNO<sub>3</sub> and 0.1 M Bu<sub>4</sub>NPF<sub>6</sub> in MeCN). Cyclic voltammograms were recorded at room temperature in dry acetonitrile, deoxygenated by bubbling with argon gas, with 0.1 M Bu<sub>4</sub>NPF<sub>6</sub> as supporting electrolyte, with ohmic drop compensation. The potentials were corrected with the ferrocene/ferrocenium redox pair (Fc/Fc<sup>+</sup>) as an internal standard, which showed the potential of 0.090–0.100 V versus the used reference electrode in our conditions. LUMO energies ( $E_{\text{LUMO}}^{\text{CV}}$ ) were estimated from the half-wave reduction potentials using the widely used relation introduced by Pommerehne et al.<sup>29</sup> (see also ref 30):  $E_{\text{LUMO}}^{\text{CV}} [\text{eV}] = -(4.8 - E_{1/2}^{\text{red}})$ , where  $-4.8$  eV is the potential of the Fc/Fc<sup>+</sup> redox pair versus the Fermi level. MEH-PPV HOMO and LUMO energies of  $-5.0$  and  $-2.8$  eV, respectively, were taken from the electrochemical data in ref 31.

**2.3. Computational Procedures.** DFT computations of the geometries of the studied fluorene electron acceptors were carried out with the Gaussian 09<sup>32</sup> package of programs by using Pople's 6-31G split valence basis set supplemented by d-polarization functions for heavy atoms and with diffusion functions on them. Becke's three-parameter hybrid exchange functional<sup>33,34</sup> with the Lee–Yang–Parr gradient-corrected correlation functional (B3LYP)<sup>35</sup> were employed. The restricted Hartree–Fock (HF) formalism was used for calculations of neutral molecules, whereas the unrestricted HF formalism was used for the calculation of radical anion states. No constraints were used and all structures were free to optimize in an acetonitrile solution using the polarizable continuum model (PCM).<sup>36–40</sup> Thus, the geometries were optimized at the B3LYP/6-31+G(d) level of theory and the electronic structures were calculated at the same level of theory. From these calculations on the neutral molecules (in acetonitrile), we estimated the frontier orbital energy levels,  $E_{\text{LUMO}}^{\text{DFT}}$  and  $E_{\text{HOMO}}^{\text{DFT}}$ . Vertical electron affinities ( $\text{EA}_V^{\text{DFT}}$ ) were computed as the difference between the total energies of the optimized neutral state  $E_{\text{total}}^{\text{OptN}}$  and the radical anion at the frozen geometry of the neutral,  $E_{\text{total}}^{\text{RA,F}}$ :

$$\text{EA}_V^{\text{DFT}} = E_{\text{total}}^{\text{OptN}} - E_{\text{total}}^{\text{RA,F}} \quad (1)$$

Adiabatic electron affinities ( $\text{EA}_A^{\text{DFT}}$ ) were calculated as the difference in total energies between the optimized geometries of the neutral  $E_{\text{total}}^{\text{OptN}}$  and radical anion  $E_{\text{total}}^{\text{RA,Opt}}$  states, including zero point energy corrections ZPE<sup>N</sup> and ZPE<sup>RA</sup> for the two states, respectively:

$$\text{EA}_A^{\text{DFT}} = E_{\text{total}}^{\text{OptN}} - E_{\text{total}}^{\text{RA,Opt}} + \text{ZPE}^N - \text{ZPE}^{\text{RA}} \quad (2)$$

**2.4. Ultrafast Spectroscopy Experiments.** The dynamics of photogenerated charges have been explored with a photoinduced absorption (PIA) technique, which allows monitoring the time evolution of photoinduced charges. The method is based on the fact that a charge (a hole) created on a polymer molecule induces absorption bands in the polymer optical gap in the IR range.<sup>41</sup> These bands called low energy (LE) and high energy (HE) polaron bands<sup>42</sup> are situated for MEH-PPV at  $\sim 3500$  and  $\sim 10\,000$  cm<sup>−1</sup>, respectively.<sup>20,43</sup> The LE band is more suitable as a reporter of charge concentration because it is not contaminated by other responses, such as electroabsorption, stimulated emission, etc., which allows for a background free measurement.<sup>20,44</sup> In the PIA technique, two pulses are applied: the first one photogenerates the charges and the second one probes the charge concentration by monitoring induced absorption in the IR spectral region. For the aforementioned reasons, the probe wavelength was set at 2.94  $\mu\text{m}$ , i.e., near the LE polaron absorption peak (see ref 20 for the polaron absorption spectrum).

Briefly, the PIA experiments were performed with a home-built 1 kHz Ti:sapphire multipass amplifier laser system that pumps an IR optical parametrical oscillator (OPO) and a nonlinear optical parametrical amplifier (NOPA). The NOPA generated  $\sim 30$  fs,  $\sim 3$  nJ pulses in the visible range (500–750 nm). The power density at the sample position did not exceed 800 nJ/cm<sup>2</sup> to ensure a linear excitation regime and the absence of bimolecular (nongeminate) recombination. The IR OPO was optimized to provide  $\sim 70$  fs pulses at  $\sim 3400$  cm<sup>−1</sup> (near the center of the LE polaron absorption band). To realize polarization-sensitive measurements, the polarization of the IR probe beam was rotated by 45° with respect to the polarization of the visible pump beam. Parallel and perpendicular components of the probe beam were selected after the sample by grid-wire polarizers and detected by two InSb photodiodes. The photodiode signals were processed by lock-in amplifiers synchronized to a mechanical chopper (500 Hz) inserted into the visible pump beam. To obtain relative changes in the transmission  $\Delta T$ , the differential pump-on, pump-off signal  $\Delta I$  from the lock-ins were normalized to the intensity  $I$  of the IR beam transmitted through the sample:

$$\Delta T = \frac{\Delta I}{I} \quad (3)$$

To calculate the isotropic  $\Delta T_{\text{Iso}}(t)$  and anisotropic  $r(t)$  transients, the standard expressions (4, 5)<sup>45</sup> were used:

$$\Delta T_{\text{Iso}}(t) = \frac{\Delta T_{\parallel}(t) + 2\Delta T_{\perp}(t)}{3} \quad (4)$$

$$r(t) = \frac{\Delta T_{\parallel}(t) - \Delta T_{\perp}(t)}{3\Delta T_{\text{Iso}}(t)} \quad (5)$$

where  $\Delta T_{\perp}(t)$  and  $\Delta T_{\parallel}(t)$  are relative transmission changes of the perpendicular and parallel components of the probe signal. All data were obtained under ambient conditions at room temperature.

### 3. RESULTS AND DISCUSSION

**3.1. Fluorene Acceptor Design.** The acceptor EA engineering was achieved by attaching a number of different electron withdrawing functional groups to the fluorene core:

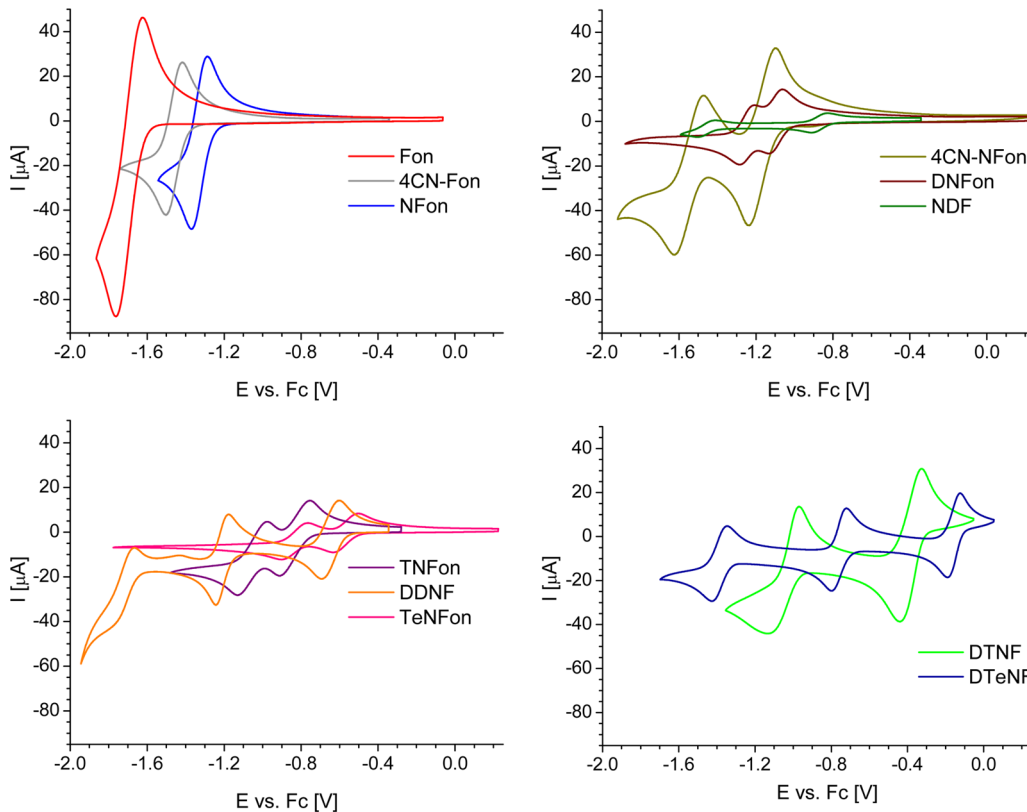


Figure 2. Cyclic voltammograms of fluorene acceptors in deoxygenated acetonitrile, supporting electrolyte 0.1 M  $\text{Bu}_4\text{NPF}_6$ , scan rate 100 mV s<sup>-1</sup>.

**Table 1. Reduction CV Potentials and Calculated Energy Levels of Fluorene Acceptors**

compound	$E_{1/2}^{\text{red1}}\text{a}$ [V]	$E_{1/2}^{\text{red2}}\text{a}$ [V]	$E_{\text{LUMO}}^{\text{CV}}\text{b}$ [eV]	$E_{\text{LUMO}}^{\text{DFT}}\text{c}$ [eV]	$E_{\text{HOMO}}^{\text{DFT}}\text{c}$ [eV]	$\text{EA}_{\text{V}}^{\text{DFTd}}$ [eV]	$\text{EA}_{\text{A}}^{\text{DFTe}}$ [eV]
Fon	-1.669	-	-3.131	-2.781	-6.534	2.891	3.140
4CN-Fon	-1.460	-	-3.340	-3.013	-6.847	3.120	3.379
4CN-NFon	-1.159	-1.516	-3.641	-3.555	-7.292	3.647	3.910
NFon	-1.328	-	-3.472	-3.372	-6.966	3.459	3.730
DNFon	-1.098	-1.245	-3.702	-3.749	-7.435	3.839	4.087
TNFon	-0.839	-1.054	-3.961	-4.045	-7.789	4.142	4.393
TeNFon	-0.564	-0.814	-4.236	-4.377	-8.136	4.478	4.725
NDF	-0.869	-1.456	-3.931	-3.768	-7.041	3.891	4.081
DDNF	-0.648	-1.210	-4.152	-4.045	-7.492	4.165	4.356
DTNF	-0.383	-1.050	-4.417	-4.302	-7.815	4.420	4.621
DTNF	-0.157	-0.760	-4.643	-4.591	-8.074	4.710	4.869

<sup>a</sup>The first and second reduction half-wave potentials in acetonitrile versus  $\text{Fc}/\text{Fc}^+$ , calculated as averages of anodic and cathodic peak potentials from cyclic voltammetry. <sup>b</sup>LUMO energy levels from CV experiments:  $E_{\text{LUMO}}^{\text{CV}} = -(4.8 - E_{1/2}^{\text{red1}})$ . <sup>c</sup>HOMO and LUMO energy levels from B3LYP/6-31+G(d) calculations in acetonitrile. <sup>d</sup>Vertical electron affinities of acceptors from B3LYP/6-31+G(d) calculations in acetonitrile (see eq 1). <sup>e</sup>Adiabatic electron affinities of acceptors from B3LYP/6-31+G(d) calculations in acetonitrile (see eq 2).

from one to four nitro groups and/or cyano group at the benzene rings, as well as using carbonyl oxygen or dicyanomethylene groups at the C-9 bridged atom of the fluorene moiety (Figure 1). While the effect of introducing several electron withdrawing groups in the fluorene moiety is not exactly additive (especially in the case of nitro groups introduced at different positions of the fluorene moiety), analysis of previous spectroscopic and electrochemical studies on different electron acceptors of the fluorene series allows for making such generalizations. The introduction of an  $\text{NO}_2$  group in substituted fluorenes increases the EA of the fluorene molecule by  $\sim 0.2\text{--}0.3$  eV, while replacement of oxygen in the carbonyl group by the dicyanomethylene fragment increases the EA by  $\sim 0.35\text{--}0.45$  eV.<sup>46–52</sup> Therefore, with the structural

variations of a selected series of fluorene acceptors presented in Figure 1, the LUMO energy levels can be tuned by  $\sim 1.5$  eV.

**3.2. Cyclic Voltammetry.** To estimate the LUMO energy levels of the studied fluorene electron acceptors, their electrochemical reduction was studied by cyclic voltammetry (CV) in dry acetonitrile, with a common three electrode scheme using  $\text{Fc}/\text{Fc}^+$  as an internal reference. Most of the studied acceptors showed two (or even three) reversible single-electron redox waves in acetonitrile solution to form stable (in CV time scale) radical anion and dianion species (or even radical trianions), respectively, except for the lowest EA acceptors Fon, 4CN-Fon, and NFon, which showed only the first redox wave to be reversible (Figure 2). An increase of the number of nitro groups results in a progressive shift of redox

potentials into the positive potential region, and further pronounced shifts are observed on replacement of O by C(CN)<sub>2</sub> groups. The first and second half-wave reduction potentials,  $E_{1/2}^{\text{red1}}$  and  $E_{1/2}^{\text{red2}}$ , are collated in Table 1 and have been used to estimate the LUMO energy levels of acceptors ( $E_{\text{LUMO}}^{\text{CV}}$ , Table 1, Figure 3), assuming an Fc potential of -4.8 eV versus

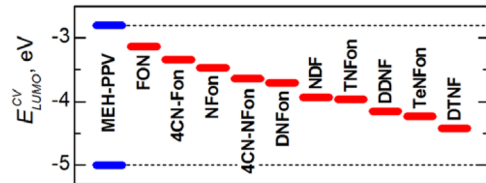


**Figure 3.** Positions of LUMO energy levels ( $E_{\text{LUMO}}^{\text{CV}}$ ) of fluorene electron acceptors from CV experiments (red blocks). MEH-PPV HOMO and LUMO energies (blue blocks) are also shown for comparison.

the Fermi level. The data for  $E_{\text{LUMO}}^{\text{CV}}$  presented in Table 1 indicate that for both series (fluorenones and 9-dicyanomethylenefluorenes) each nitro group incrementally decreases the LUMO energy of the acceptors by ~0.22–0.27 eV, except for the weakest acceptor, unsubstituted fluorenone Fon, in which case an insertion of the first NO<sub>2</sub> group (NFon) results in a decrease of the LUMO energy by 0.34 eV. Replacement of carbonyl oxygen by dicyanomethylene group in acceptors decreases their LUMO energies by 0.41–0.46 eV. These data are in good agreement with the observed linear relationships of first reduction potentials,<sup>53</sup> as well as of intramolecular charge transfer energies<sup>54</sup> in fluorene acceptors by Hammett-type correlations. The EAs of the studied acceptors estimated from the electrochemical experiments were assigned as  $\text{EA}^{\text{CV}} = -E_{\text{LUMO}}^{\text{CV}}$  in accordance with Koopman's theorem.

**3.3. DFT Computational Studies.** DFT computations have been performed at the B3LYP/6-31+G(d) level of theory for both geometry optimizations and calculations of electronic structures of neutral acceptors and their radical anions. The effect of the solvent (acetonitrile) was incorporated using the polarizable continuum model (PCM) to match the results with CV measurements in this solvent. Kohn–Sham frontier orbital energies for neutral acceptors,  $E_{\text{HOMO}}^{\text{DFT}}$  and  $E_{\text{LUMO}}^{\text{DFT}}$ , are collated in Table 1 (more details on the B3LYP/6-31+G(d) level of theory calculations are given in Supporting Information, Table S1). Orbital energy diagrams together with HOMO and LUMO orbital coefficients of the fluorene acceptors obtained from B3LYP/6-31+G(d) calculations in acetonitrile are given in the Supporting Information (Figure S18 and Table S2). It is evident that nitro groups incrementally decrease the LUMO energy levels for both fluorenone and 9-dicyanomethylene series of acceptors (Supporting Information, Figure S18), and while their effect is not fully additive, the trend is clear and in general reproduces well the observations of CV experiments. Both nitro groups and the dicyanomethylene fragment are substantially involved in LUMO delocalization, with a more pronounced effect for the NO<sub>2</sub> groups in positions 2,7 as compared to positions 4,5. Cyano groups in the benzene ring are very weakly involved in the LUMO delocalization (Figure 4, Supporting Information, Table S2). The lower degree of LUMO delocalization over the 4,5-nitro groups is partially due to a steric effect. According to single crystal X-ray data for various fluorene acceptors and their CTC, this results in rotation of NO<sub>2</sub> around the C–N bond to form dihedral angles

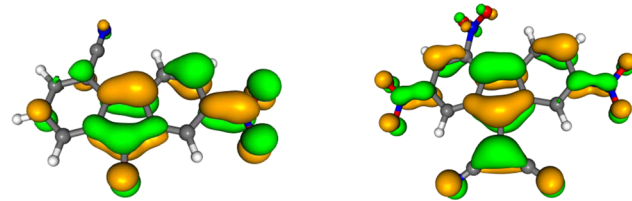


**Figure 4.** LUMO orbital coefficients for two representative fluorene acceptors from B3LYP/6-31+G(d) calculations in acetonitrile. For others, see the Supporting Information, Table S2.

with the fluorene plane (in general, 30–50° and 3–10° for nitro groups in positions 4,5 and 2,7, respectively<sup>48–53,55–60</sup>).

In the DFT calculations, EAs are sometimes approximated by the LUMO energies ( $\text{EA} = -E_{\text{LUMO}}$ ) in accordance with DFT–Koopman's theorem. In addition to such an estimation, we also calculated vertical and adiabatic electron affinities,  $\text{EA}_V^{\text{DFT}}$  and  $\text{EA}_A^{\text{DFT}}$  (Table 1). Both vertical and adiabatic EA values are in excellent linear relationships with the computed  $E_{\text{LUMO}}^{\text{DFT}}$  energies, while a better coincidence in absolute values is observed with the vertical ionization potentials,  $\text{EA}_V^{\text{DFT}}$  (average deviation is of ca. -0.1 eV; see Figure 5 and the Supporting

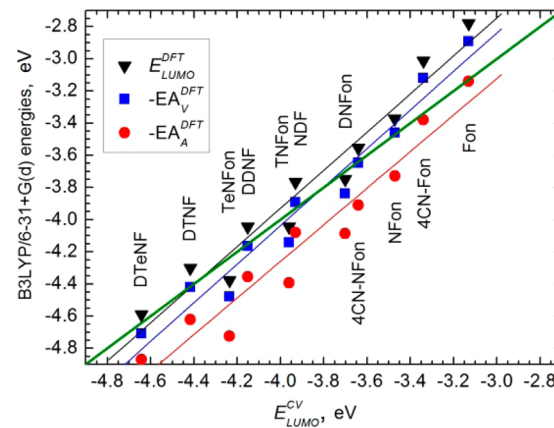


**Figure 5.** Comparison of experimental and calculated B3LYP/6-31+G(d) LUMO energy levels (ionization potentials) for the studied electron acceptors. Green line represents a bisection of equal energies between the axes (as such, the best quantitative coincidence with experimental data is for  $\text{EA}_V^{\text{DFT}}$  calculated values). Solid lines show linear fits to the respective data sets.

Information, Figures S19 and S20). Comparison of the DFT data with CV experiments indicates that  $E_{\text{LUMO}}^{\text{DFT}}$  and  $\text{EA}_V^{\text{DFT}}$  show reasonably good linear correlations with the experimental  $E_{\text{LUMO}}^{\text{CV}}$  values obtained from the cyclic voltammetry experiments, while for  $\text{EA}_A^{\text{DFT}}$  the deviations are somewhat larger (Figure 5). In all cases, the slopes are slightly higher than unity and increased positive deviations are observed for weaker acceptors Fon and 4CN-Fon, implying an underestimation of the EA by the DFT calculations. Small deviations from linear dependence between the CV data and computational estimations of orbital energies are partially due to the known fact of overestimation of conjugation by global hybrid functionals<sup>61–65</sup> affecting the computed LUMO energies as well as adiabatic EA values. Yet, reasonably good linear correlations between the experiments and the theory allow using computational methods in the design of fluorene

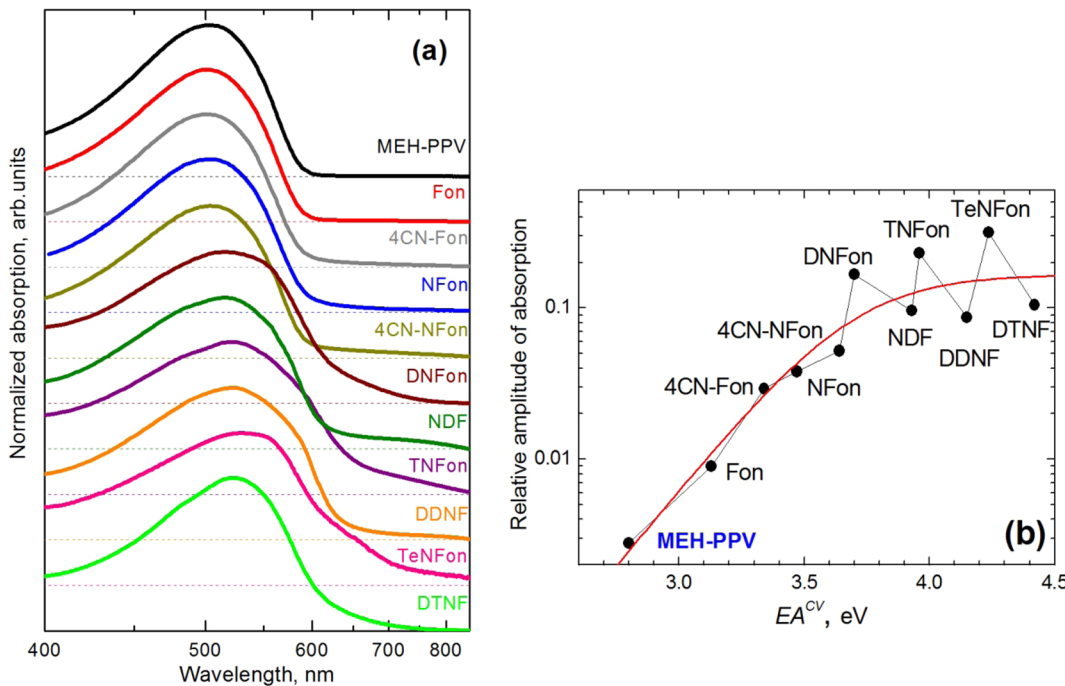


**Figure 6.** (a) Normalized absorption spectra for MEH-PPV:acceptor films. The spectra are shifted vertically for clarity; the acceptor EA increases from top to bottom. The spectrum of a pristine MEH-PPV film is also shown at the top for comparison. (b) Absorption at the red tail of the spectrum (650 nm; chosen arbitrarily) relative to the maximum absorption as a function of acceptor EA. The red curve shows the fit to an ad hoc function  $A(\exp(-b \cdot EA) + c)^{-1}$  to highlight the initial exponential growth followed by the saturation.

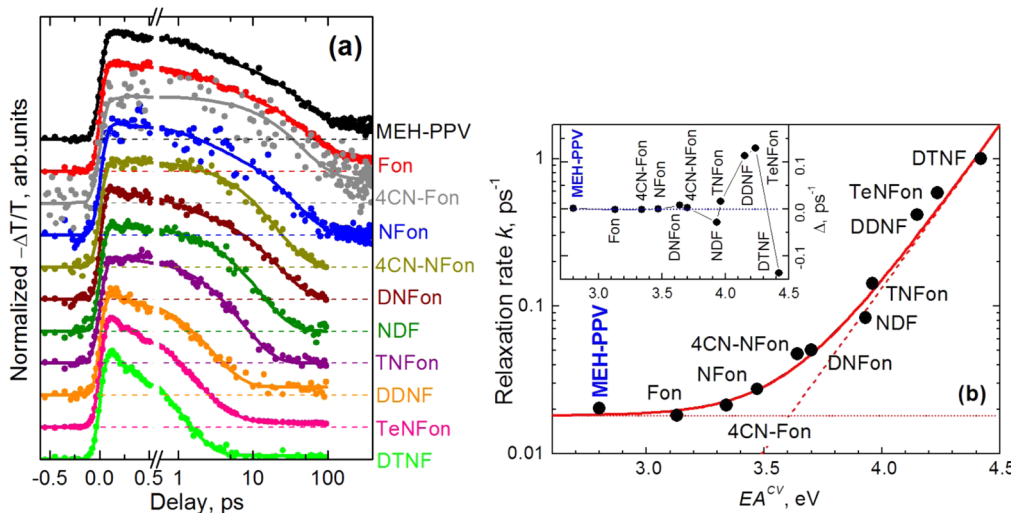


**Figure 7.** (a) Normalized isotropic PIA transients for MEH-PPV:acceptor blends at an excitation wavelength of 560 nm and probe wavelength of  $2.94 \mu\text{m}$ . Dots represent experimental data, while solid curves show biexponential fits with the parameters listed in Table S3 in the Supporting Information. The transients are shifted vertically for clarity; the corresponding zero signal levels are shown by dashed lines. Note the logarithmic scaling of the delay axis after the break. The PIA signal from the pristine MEH-PPV film (black) is shown as a reference. (b) Charge recombination rate in blends of MEH-PPV:acceptor as a function of EA. The solid curve represents the best fit to the experimental data (dots) according to eq 6. The dashed and dotted lines are asymptotes for the acceptor-to-polymer and intrapolymer recombination channels, respectively. The inset presents deviations of the experimental values from the best fit at the linear scale.

acceptors with predictable EAs. Therefore, in the following we will use  $-E_{\text{LUMO}}^{\text{CV}}$  as the acceptor EA.

**3.4. Steady-State Absorption.** Figure 6a plots optical absorption spectra of the MEH-PPV:acceptor blends. For the sake of simplicity, the blends are named after the respective acceptor. With increase of the acceptor EA, i.e., with lowering of the effective HOMO–LUMO energy gap, the blends show characteristic signatures of a ground-state polymer:acceptor

CTC previously identified for MEH-PPV:TNFon blends.<sup>8,13</sup> First, an absorption tail begins to form in the polymer band gap, i.e., at wavelengths longer than 600 nm (Figure 6b). Second, the absorption maximum is progressively shifted to the red (Figure 6a) for acceptors with EA higher than that of 4CN-NFon. This indicates that the majority of the conjugated chains are involved in the CTC.<sup>13</sup> For acceptors with high EA, an additional CTC absorption band is formed (most clearly seen

for TeNFon), in accordance with the Mulliken model which predicts that the CTC absorption should be progressively red-shifted with increasing of the acceptor EA.

The absorption spectra in Figure 6a indicate that the polymer forms easily observable CTCs with the acceptors having an EA equal to or higher than that for DNFon. For acceptors with a relatively low EA (4CN-NFon, NFon, 4CN-Fon, and Fon), the only CTC signature is a weak absorption in the polymer gap (Figure 6b) that increases exponentially with acceptor EA. Interestingly, the CTC absorption ceases to be a monotonic function of EA at the position of DNFon. As follows from Figure 6b, the fluorenone acceptors (i.e., with carbonyl oxygen at the C-9 bridged atom of the fluorene moiety, Figure 1) form stronger absorbing CTCs than their dicyanomethylenefluorene-derivatized counterparts with comparable EAs (cf. for pairs NDF/TNFon and DDNF/TeNFon). Therefore, EA is not the only variable that governs the CTC properties even for acceptors with similar molecular structures.

**3.5. Photoinduced Charge Generation and Recombination.** While absorption data are indispensable in studying the formation of the ground-state CTCs, they do not provide any information on the excited-state dynamics, i.e., on the processes of charge separation and recombination. For this, a visible-pump–IR-probe arrangement<sup>20</sup> was used where the magnitude of PIA signals in the region of LE polaron absorption (at 2.94 μm) monitors the concentration of photoinduced charges on the polymer.

Figure 7 shows isotropic PIA transients for all the MEH-PPV:acceptor blends recorded at an excitation wavelength of 560 nm. This excitation wavelength was chosen at the lower-energy side of the absorption spectra (Figure 6a) to minimize deposition of excessive excitation energy. As is clear from Figure 7a, the initial charge photogeneration for all the samples is extremely fast and occurs within the apparatus time resolution of ~100 fs, regardless of the acceptor. Therefore, we conclude that the polaron generation in the blends occurs faster than 100 fs, and hence forward donor-to-acceptor electron transfer is almost immediate upon optical excitation and does not depend on the driving force for charge separation (acceptor EA). In contrast, the decaying parts of the transients are strongly acceptor dependent with the relaxation time scale changing from ~50 ps for Fon to ~1 ps for DTNF. These time scales are attributed to the charge recombination (or back electron transfer from the acceptor to the polymer) process.

We briefly comment on the origin of the PIA signal from the film of pristine MEH-PPV. Ideally, such excitation should be of entirely excitonic nature so that almost no polarons are produced. However, a number of MEH-PPV excitons quickly dissociate into charge species whose assignment was actively debated in the past (see, for instance, ref 66). Here we use the PIA signal from the pristine MEH-PPV film only as a reference for the charge recombination in the blends not affected by CTC formation.

To quantify the dynamics, the transients were fitted by a biexponential function (Figure 7a, solid lines) with fit parameters presented in the Supporting Information (see Table S3). Two recombination rates most probably correspond to different donor–acceptor configurations and/or partial electron transfer. In any case, for the majority of the acceptors, the amplitude of the dominating exponential functions exceeds 90% and is always higher than 80%. We took the weighted average of the two time constants as the characteristic time of the charge recombination.

Figure 7b summarizes the relation between the charge recombination rate,  $k$ , and the acceptor EA. The intermolecular recombination rate mostly follows the exponential trend with some deviations for low-EA acceptors. This deviation originates from a second, intrapolymer (i.e., between units of the same and/or different polymer chains) channel of charge recombination that is characteristic for pristine MEH-PPV. The charge recombination rate that accounts for the both donor–acceptor and intrapolymer channels is therefore expressed as follows:

$$k = k_{ET} \left[ \exp\left(\frac{EA}{\Delta E}\right) - 1 \right] + k_0 \quad (6)$$

where  $k_{ET}$  is the proportionality coefficient,  $\Delta E$  is a characteristic energy, and  $k_0$  is the rate of the intrapolymer charge recombination. The fit to the experimental data resulted in the following values:  $k_{ET} = 2.1 \times 10^{-10} \text{ ps}^{-1}$ ,  $\Delta E = 0.2 \text{ eV}$ , and  $k_0 = 0.018 \text{ ps}^{-1}$ .

The linear dependence of the logarithm of the charge recombination rate,  $\ln(k)$ , on EA has been observed in many small-molecule ground-state CTCs, both in solution<sup>6,7</sup> and in the solid phase.<sup>26,67</sup> The obtained value of  $\Delta E^{-1} = 5 \text{ eV}^{-1}$  of the slope of the exponential factor is also similar to values from previous studies of small-molecule CTCs. For instance, Gould et al.<sup>6</sup> reported the slope value of ~5 eV<sup>-1</sup> in a series of CTCs formed between cyanoaromatic acceptors and methyl-substituted benzene donors. Hubig et al. found<sup>7,26</sup> the slope to vary from 2 eV<sup>-1</sup> in benzene–methylviologen mixtures up to 3.6 eV<sup>-1</sup> in CTCs between large aromatics and TCNB (tetracyanobenzene) acceptor.

In the Marcus model,<sup>68</sup> an increase of the charge recombination rate with increasing EA (the driving force) corresponds to the so-called inverted regime.<sup>69–71</sup> Various interpretations of the Marcus model were proposed to obtain a linear dependence of the experimentally observed  $\ln(k)$  on EA for charge recombination in various small-molecule CTCs. As follows from the Marcus equation,<sup>68</sup> such a linear dependence of  $\ln(k)$  appears when the reorganization energy becomes much larger than the driving force for charge recombination. As the latter is always higher than 0.5 eV for the examined CTCs, this leads in our case to an unreasonably high reorganization energy, by a factor of 5 higher than imposed by  $kT$ . On the other hand, the linear EA dependence of  $\ln(k)$  can be assigned to the energy gap law for radiationless transitions in polyatomic molecules as was explained for small-molecule CTCs adsorbed on porous glass at different temperatures.<sup>67</sup> These are quantum transitions between (nearly) degenerated vibrational levels that belong to the ground and excited electronic states of the molecule<sup>72</sup> (that is a photoexcited CTC in our case). Note that these transitions are not thermally activated as the classic Marcus model implies (for a detailed discussion of the inverted Marcus and the energy gap models, see refs 69 and 70). Therefore, we suggest that in the conjugated polymer CTCs the charge recombination mechanism is very similar to that observed earlier in small-molecule CTCs.

The data in Figure 7a suggest that the acceptor EA is the prime factor that governs the charge recombination rate for the CTCs used herein. Nonetheless, the fluorenone acceptors are characterized by slightly higher relaxation rates than the dicyanomethylenefluorene ones of similar EAs (compare, for instance, pairs of NDF/TNFon and DDNF/TeNFon). This shows that other CTC parameters, such as the molecular orbital

overlap, the donor–acceptor distances, the packing motif, etc. that enter the pre-exponential factor in eq 6, are also important.

From Figure 7b one can readily establish the EA (which is, in the first approximation, directly linked to the driving force for charge recombination) where the donor–acceptor recombination channel begins to dominate over the intrapolymer one ( $\sim 50$  ps for pristine MEH-PPV). This energy can be estimated by equalizing the rates of donor–acceptor and intrapolymer charge transfer, i.e., as the abscissa of the crossing point between the dashed and dotted lines in Figure 6b, which results in  $\sim 3.6$  eV.

Figure 8 presents PIA anisotropy transients for the MEH-PPV:acceptor blends. The initial anisotropy value of  $\sim 0.3$  is

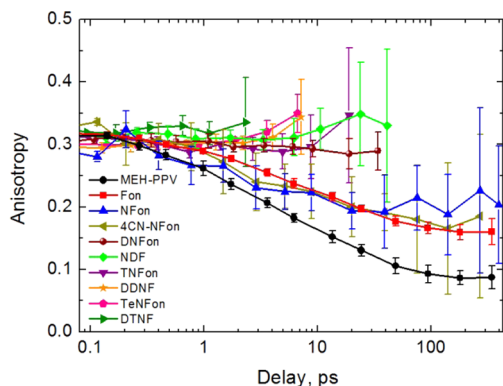


**Figure 8.** PIA anisotropy transients for MEH-PPV:acceptor blends at an excitation wavelength of 560 nm and probe wavelength of  $2.94 \mu\text{m}$ . The transients are delay-limited because of deteriorating signal-to-noise ratio due to short lifetimes in the blends with high-EA acceptors.

virtually independent of the acceptor. This means that the transient dipoles of photoexcitation (i.e., blend absorption) and probe (i.e., polaron absorption) remain unaffected by CTC formation. The long-time behavior strongly depends on the acceptor: for DNFon and acceptors with higher EAs the transient anisotropy does not change appreciably from its initial value. In contrast, for the acceptors with lower EAs (Fon, NFon, and 4CN-NFon), the anisotropy decreases with time in a similar fashion as for MEH-PPV, although to a lower extent. The anisotropy dynamics are ascribed to polaron migration on the polymer: as the polaron samples polymer segments with various orientations, the memory of the initial direction of the polaron transition dipole moment is more and more lost. Therefore, we conclude that the polarons are more mobile in the blends with acceptors of low EAs, while they are more localized in the blends with the acceptors of higher EAs. The borderline, as found above in the isotropic PIA and steady-state spectroscopy data, is drawn at the EA of the DNFon acceptor.

Based on our optical experiments, we propose the following model of charge dynamics in polymer–acceptor blends with ground-state CTCs (Figure 9). For low-EA acceptors, namely Fon, NFon, and 4CN-NFon, the CTC concentration in the polymer phase is relatively low while the majority of acceptor molecules form their own phase (Figure 9a). As a consequence, a part of the photoexcitations that are characteristic of pristine polymer is mobile, but another part—those of CTCs—is localized. The fraction of the former decreases for acceptors with high EAs which results in the red-wing absorption (Figure 6a), accelerated recombination rate (Figure 7), and lowered anisotropy values (Figure 8). Acceptors with high EAs form

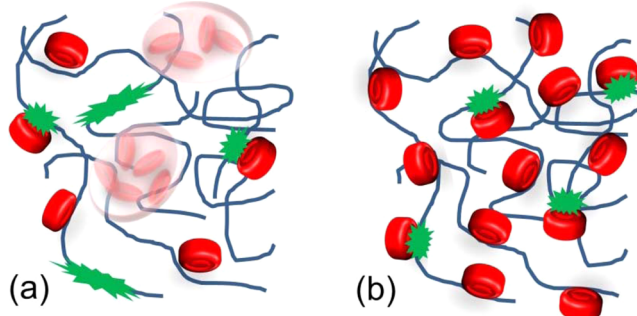


**Figure 9.** Impression of MEH-PPV:acceptor blend charge dynamics for acceptors with (a) low and (b) high EAs. Very few low-EA acceptors form CTCs (red pucks) with polymer chains (blue), while most acceptors aggregate in their own phase (shadowed in light red). This results in mobile (extended green) and more localized (green) photoexcitations. In contrast, almost all high-EA acceptors form CTCs with polymer chains resulting in localized excitations only.

CTCs that are more dispersed in the conjugated polymer (Figure 9b; see also discussion on the absorption spectra, Figure 6) so that a polymer photoexcitation always occurs near an acceptor molecule that immediately receives the photo-excited electron. Such complexation, in turn, planarizes MEH-PPV segments thereby increasing the conjugation length within these fragments of the polymer backbone<sup>73</sup> (and consequently delocalization of the photoexcitation) that in turn facilitates an efficient charge separation processes. As a consequence, the polaron stays in the vicinity of its birthplace, which results in a time-independent anisotropy. Note that in this case the intrapolymer recombination channel (the second term in eq 6) becomes irrelevant and therefore the recombination rates approach the exponential behavior (Figure 7b). Most probably, the previously observed self-organization of the polymer chains in crystalline domains due to the CTC formation<sup>14</sup> adds another dimension to this scenario; a more detailed investigation on this issue is underway.

#### 4. CONCLUSIONS

The ground-state CTCs formed between a conjugated polymer donor (MEH-PPV) and a series of fluorene electron acceptors with varying electron affinity have been studied using a combined platform of synthetic chemistry, DFT calculations, and time-resolved spectroscopy. The acceptor EAs were engineered by attaching a variety of electron withdrawing functional groups (cyano, nitro, and carbonyl) to the fluorene core to systematically modify the LUMO energies of the acceptors. Acceptor frontier orbital energies were calculated using a DFT method at the B3LYP/6-31+G(d) level of theory and compared with measurements of acceptors' electrochemical reduction potentials obtained from cyclic voltammetry. The experimental and theoretical values demonstrated excellent agreement.

The formation of the ground-state CTCs in polymer–acceptor blends has been identified by optical absorption spectroscopy through the appearance of an additional absorption in the polymer band gap. Visible-IR PIA spectroscopy has been further employed to study excited-state charge separation and recombination dynamics. In all the blends, charge photogeneration is extremely fast ( $< 100$  fs), while charge recombination shows noticeably different dynamics ranging from 1 to 50 ps. The acceptor-to-polymer recombi-

tion rates exhibit an exponential scaling with the acceptor EA with parameters that are similar to those reported earlier for small-molecule CTCs. Transient anisotropy data have indicated that, in the CTCs with acceptors of relatively high EA, the mutual orientation of photoexcited and polaron transient dipole moments is retained, whereas in the low-EA acceptors the two dipole moments become less correlated.

The experimental data have been discussed in terms of a charge dynamics model where the low-EA acceptors form relatively sparse CTCs with the polymer chain and most of the acceptor molecules stay phase separated from the polymer. In contrast, the high-EA acceptors are thought to be rather dispersed in the polymer due to pronounced CTC formation. As a result, in the first case photoexcitations are fractioned between delocalized polymeric and more localized CTCs ones while in the second case photoexcitations are localized around the point of their creation.

The effect of the acceptor EA on the charge recombination dynamics has clear implications for organic solar cells. The charge-transfer state with the hole at the donor and the electron at the acceptor, both near the interface, has been recognized as a key intermediate state on the route from photon absorption to free charges in various donor–acceptor combinations.<sup>31,42,74</sup> Our results demonstrate that acceptors with a higher EA (i.e., those providing a stronger driving force for charge separation) result in an exponentially increased recombination rate from the CTC state which leads to reduction of the long-lived separated charges. These two opposite trends should be carefully balanced in designing the novel organic bulk heterojunctions.

## ASSOCIATED CONTENT

### Supporting Information

Synthesis and characterization of studied fluorene acceptors with respective <sup>1</sup>H and <sup>13</sup>C NMR spectra, UV–visible absorption spectra of the acceptors, DFT calculations for fluorene acceptors and correlations between computational DFT data and CV experiments, fitting parameters for ultrafast spectroscopy data. This material is available free of charge via the Internet at <http://pubs.acs.org>.

## AUTHOR INFORMATION

### Corresponding Authors

\*E-mail: M.S.Pchenitchnikov@rug.nl (M.S.P.).

\*E-mail: i.perepichka@bangor.ac.uk (I.F.P.).

### Present Addresses

<sup>1</sup>M.K.: Merck Chemicals Ltd., Chilworth Technical Centre, University Parkway, Southampton, SO16 7QD, U.K.

<sup>#</sup>P.H.M.L.: II. Physikalisches Institut, Universität zu Köln, 50923 Köln, Germany.

### Author Contributions

The manuscript was written through contributions of all authors. All authors have given approval to the final version of the manuscript.

### Notes

The authors declare no competing financial interest.

## ACKNOWLEDGMENTS

O.D.P. and D.Yu.P. acknowledge the partial support of the Russian Foundation for Basic Research (RFBR No. 13-03-12472 and No. 13-02-01313) and the M. V. Lomonosov Moscow State University Program of Development. We thank

A. Serbenta for performing some measurements on optical absorption and ultrafast dynamics. A. A. Bakulin and D. Beljonne are acknowledged for many useful discussions.

## REFERENCES

- (1) Mulliken, R. S. Structures of Complexes Formed by Halogen Molecules with Aromatic and with Oxygenated Solvents. *J. Am. Chem. Soc.* **1950**, *72*, 600–608.
- (2) Mulliken, R. S. Molecular Compounds and Their Spectra. II. *J. Am. Chem. Soc.* **1952**, *74*, 811–824.
- (3) Veldman, D.; Meskers, S. C. J.; Janssen, R. A. J. The Energy of Charge-Transfer States in Electron Donor-Acceptor Blends: Insight into the Energy Losses in Organic Solar Cells. *Adv. Funct. Mater.* **2009**, *19*, 1939–1948.
- (4) Hwang, I. W.; Moses, D.; Heeger, A. J. Photoinduced Carrier Generation in P3HT/PCBM Bulk Heterojunction Materials. *J. Phys. Chem. C* **2008**, *112*, 4350–4354.
- (5) Veldman, D.; Ipek, O.; Meskers, S. C. J.; Sweelssen, J.; Koetse, M. M.; Veenstra, S. C.; Kroon, J. M.; van Bavel, S. S.; Loos, J.; Janssen, R. A. J. Compositional and Electric Field Dependence of the Dissociation of Charge Transfer Excitons in Alternating Polyfluorene Copolymer/Fullerene Blends. *J. Am. Chem. Soc.* **2008**, *130*, 7721–7735.
- (6) Gould, I. R.; Noukakis, D.; Gomejahn, L.; Young, R. H.; Goodman, J. L.; Farid, S. Radiative and Nonradiative Electron-Transfer in Contact Radical-Ion Pairs. *Chem. Phys.* **1993**, *176*, 439–456.
- (7) Hubig, S. M.; Bockman, T. M.; Kochi, J. K. Optimized Electron Transfer in Charge-Transfer Ion Pairs. Pronounced Inner-Sphere Behavior of Olefin Donors. *J. Am. Chem. Soc.* **1996**, *118*, 3842–3851.
- (8) Bakulin, A. A.; Elizarov, S. G.; Khodarev, A.; Martyanov, D. S.; Golovnin, I.; Paraschuk, D. Y.; Triebel, M. M.; Tolstov, I.; Bruevich, E. L.; Arnaudov, S. A.; et al. Weak Charge-Transfer Complexes Based on Conjugated Polymers for Plastic Solar Cells. *Synth. Met.* **2004**, *147*, 221–225.
- (9) Goris, L.; Haenen, K.; Nesladek, M.; Wagner, P.; Vanderzande, D.; De Schepper, L.; D'Haen, J.; Lutsen, L.; Manca, J. V. Absorption Phenomena in Organic Thin Films for Solar Cell Applications Investigated by Photothermal Deflection Spectroscopy. *J. Mater. Sci.* **2005**, *40*, 1413–1418.
- (10) Panda, P.; Veldman, D.; Sweelssen, J.; Bastiaansen, J. J. A. M.; Langeveld-Voss, B. M. W.; Meskers, S. C. J. Charge Transfer Absorption for  $\pi$ -Conjugated Polymers and Oligomers Mixed with Electron Acceptors. *J. Phys. Chem. B* **2007**, *111*, 5076–5081.
- (11) Wise, A. J.; Grey, J. K. Resonance Raman Studies of Excited State Structural Displacements of Conjugated Polymers in Donor/Acceptor Charge Transfer Complexes. *Phys. Chem. Chem. Phys.* **2012**, *14*, 11273–11276.
- (12) Sosorev, A. Y.; Paraschuk, D. Y. Charge-Transfer Complexes of Conjugated Polymers. *Isr. J. Chem.* **2014**, *54*, 650–673.
- (13) Bruevich, V. V.; Makhmutov, T. S.; Elizarov, S. G.; Nechvolodova, E. M.; Paraschuk, D. Y. Raman Spectroscopy of Intermolecular Charge Transfer Complex between a Conjugated Polymer and an Organic Acceptor Molecule. *J. Chem. Phys.* **2007**, *127*, 104905.
- (14) Paraschuk, O. D.; Grigorian, S.; Levin, E. E.; Bruevich, V. V.; Bukanov, K.; Golovnin, I. V.; Dittrich, T.; Dembo, K. A.; Volkov, V. V.; Paraschuk, D. Y. Acceptor-Enhanced Local Order in Conjugated Polymer Films. *J. Phys. Chem. Lett.* **2013**, *4*, 1298–1303.
- (15) Bruevich, V. V.; Makhmutov, T. S.; Elizarov, S. G.; Nechvolodova, E. M.; Paraschuk, D. Y. Ground State of  $\pi$ -Conjugated Polymer Chains Forming an Intermolecular Charge-Transfer Complex as Probed by Raman Spectroscopy. *J. Exp. Theor. Phys.* **2007**, *105*, 469–478.
- (16) Benson-Smith, J. J.; Goris, L.; Vandewal, K.; Haenen, K.; Manca, J. V.; Vanderzande, D.; Bradley, D. D. C.; Nelson, J. Formation of a Ground-State Charge-Transfer Complex in Polyfluorene/[6,6]-Phenyl-C<sub>61</sub> Butyric Acid Methyl Ester (PCBM) Blend Films and Its

- Role in the Function of Polymer/PCBM Solar Cells. *Adv. Funct. Mater.* **2007**, *17*, 451–457.
- (17) Drori, T.; Sheng, C. X.; Ndobe, A.; Singh, S.; Holt, J.; Vardeny, Z. V. Below-Gap Excitation of  $\pi$ -Conjugated Polymer–Fullerene Blends: Implications for Bulk Organic Heterojunction Solar Cells. *Phys. Rev. Lett.* **2008**, *101*, 037401.
- (18) Goris, L.; Poruba, A.; Hodyakova, L.; Vanecek, M.; Haenen, K.; Nesladek, M.; Wagner, P.; Vanderzande, D.; De Schepper, L.; Manca, J. V. Observation of the Subgap Optical Absorption in Polymer–Fullerene Blend Solar Cells. *Appl. Phys. Lett.* **2006**, *88*, 052113.
- (19) Hallermann, M.; Haneder, S.; Da Como, E. Charge-Transfer States in Conjugated Polymer/Fullerene Blends: Below-Gap Weakly Bound Excitons for Polymer Photovoltaics. *Appl. Phys. Lett.* **2008**, *93*, 053307.
- (20) Bakulin, A. A.; Martyanov, D. S.; Paraschuk, D. Y.; Pshenichnikov, M. S.; van Loosdrecht, P. H. M. Ultrafast Charge Photogeneration Dynamics in Ground-State Charge-Transfer Complexes Based on Conjugated Polymers. *J. Phys. Chem. B* **2008**, *112*, 13730–13737.
- (21) Bakulin, A. A.; Martyanov, D.; Paraschuk, D. Y.; van Loosdrecht, P. H. M.; Pshenichnikov, M. S. Charge-Transfer Complexes of Conjugated Polymers as Intermediates in Charge Photogeneration for Organic Photovoltaics. *Chem. Phys. Lett.* **2009**, *482*, 99–104.
- (22) He, Z.; Zhong, C.; Su, S.; Xu, M.; Wu, H.; Cao, Y. Enhanced Power-Conversion Efficiency in Polymer Solar Cells Using an Inverted Device Structure. *Nat. Photonics* **2012**, *6*, 591–595.
- (23) Liang, Y.; Xu, Z.; Xia, J.; Tsai, S.-T.; Wu, Y.; Li, G.; Ray, C.; Yu, L. For the Bright Future—Bulk Heterojunction Polymer Solar Cells with Power Conversion Efficiency of 7.4%. *Adv. Mater.* **2010**, *22*, 135–138.
- (24) van Mullekom, H. A. M.; Vekemans, J. A. J. M.; Havinga, E. E.; Meijer, E. W. Developments in the Chemistry and Band Gap Engineering of Donor–Acceptor Substituted Conjugated Polymers. *Mater. Sci. Eng., R* **2001**, *32*, 1–40.
- (25) Blayney, A. J.; Perepichka, I. F.; Wudl, F.; Perepichka, D. F. Advances and Challenges in the Synthesis of Poly(p-phenylene vinylene)-Based Polymers. *Isr. J. Chem.* **2014**, *54*, 674–688.
- (26) Hubig, S. M.; Kochi, J. K. Photoinduced Electron Transfer in Charge-Transfer Crystals by Diffuse-Reflectance (Picosecond) Time-Resolved Spectroscopy. *J. Phys. Chem.* **1995**, *99*, 17578–17585.
- (27) Bakulin, A. A.; Khodarev, A. N.; Martyanov, D. S.; Elizarov, S. G.; Golovnin, I. V.; Paraschuk, D. Yu.; Arnautov, S. A.; Nechvolodova, E. M. Charge Transfer Complexes of a Conjugated Polymer. *Doklady Chemistry* **2004**, *398*, 204–206.
- (28) Elizarov, S. G.; Ozimova, A. E.; Paraschuk, D. Y.; Arnautov, S. A.; Nechvolodova, E. M. Laser Light Scattering as a Probe of Phase Separation in Conjugated Polymer Films of Donor-Acceptor Blends. *Proc. SPIE* **2006**, *6257*, 293–302.
- (29) Pommerehne, J.; Vestweber, H.; Guss, W.; Mahrt, R. F.; Bässler, H.; Porsch, M.; Daub, J. Efficient 2-Layer LEDs on a Polymer Blend Basis. *Adv. Mater.* **1995**, *7*, 551–554.
- (30) Cardona, C. M.; Li, W.; Kaifer, A. E.; Stockdale, D.; Bazan, G. C. Electrochemical Considerations for Determining Absolute Frontier Orbital Energy Levels of Conjugated Polymers for Solar Cell Applications. *Adv. Mater.* **2011**, *23*, 2367–2371.
- (31) Brabec, C. J.; Sariciftci, N. S.; Hummelen, J. C. Plastic Solar Cells. *Adv. Funct. Mater.* **2001**, *11*, 15–26.
- (32) Frisch, M. J.; Trucks, G. W.; Schlegel, H. B.; Scuseria, G. E.; Robb, M. A.; Cheeseman, J. R.; Scalmani, G.; Barone, V.; Mennucci, B.; Petersson, G. A.; Nakatsuji, H.; et al., *Gaussian 09*, revision A02; Gaussian, Inc.: Wallingford, CT, 2009.
- (33) Becke, A. D. Density-Functional Exchange-Energy Approximation with Correct Asymptotic-Behavior. *Phys. Rev. A* **1988**, *38*, 3098–3100.
- (34) Becke, A. D. Density-Functional Thermochemistry: 3. The Role of Exact Exchange. *J. Chem. Phys.* **1993**, *98*, 5648–5652.
- (35) Lee, C.; Yang, W.; Parr, R. G. Development of the Colle-Salvetti Correlation-Energy Formula into a Functional of the Electron-Density. *Phys. Rev. B* **1988**, *37*, 785–789.
- (36) Barone, V.; Cossi, M.; Tomasi, J. A New Definition of Cavities for the Computation of Solvation Free Energies by the Polarizable Continuum Model. *J. Chem. Phys.* **1997**, *107*, 3210–3221.
- (37) Cammi, R.; Tomasi, J. Analytical Derivatives for Molecular Solutes: 1. Hartree-Fock Energy First Derivatives with Respect to External Parameters in the Polarizable Continuum Model. *J. Chem. Phys.* **1994**, *100*, 7495–7502.
- (38) Miertus, S.; Scrocco, E.; Tomasi, J. Electrostatic Interaction of a Solute with a Continuum—a Direct Utilization of Ab initio Molecular Potentials for the Revision of Solvent Effects. *Chem. Phys.* **1981**, *55*, 117–129.
- (39) Tomasi, J.; Persico, M. Molecular-Interactions in Solution—an Overview of Methods Based on Continuous Distributions of the Solvent. *Chem. Rev.* **1994**, *94*, 2027–2094.
- (40) Tomasi, J.; Mennucci, B.; Cammi, R. Quantum Mechanical Continuum Solvation Models. *Chem. Rev.* **2005**, *105*, 2999–3093.
- (41) Mizrahi, U.; Shtrichman, I.; Gershoni, D.; Ehrenfreund, E.; Vardeny, Z. V. Picoseconds Time Resolved Photoinduced Absorption by Infrared Active Vibrations as a Probe for Charge Photogeneration in MEH-PPV/C-60 Composites. *Synth. Met.* **1999**, *102*, 1182–1185.
- (42) Sariciftci, N. S.; Smilowitz, L.; Heeger, A. J.; Wudl, F. Photoinduced Electron-Transfer from a Conducting Polymer to Buckminsterfullerene. *Science* **1992**, *258*, 1474–1476.
- (43) Lane, P. A.; Wei, X.; Vardeny, Z. V. Studies of Charged Excitations in  $\pi$ -Conjugated Oligomers and Polymers by Optical Modulation. *Phys. Rev. Lett.* **1996**, *77*, 1544–1547.
- (44) Osterbacka, R.; Wohlgemant, M.; Shkunov, M.; Chinn, D.; Vardeny, Z. V. Excitons, Polarons, and Laser Action in Poly(p-phenylene vinylene) Films. *J. Chem. Phys.* **2003**, *118*, 8905–8916.
- (45) Gordon, R. G. Molecular Collisions and Depolarization of Fluorescence in Gases. *J. Chem. Phys.* **1966**, *45*, 1643–1655.
- (46) Mysyk, D. D.; Perepichka, I. F.; Perepichka, D. F.; Bryce, M. R.; Popov, A. F.; Goldenberg, L. M.; Moore, A. J. Electron Acceptors of the Fluorene Series. 9. Derivatives of 9-(1,2-Dithiol-3-ylidene)-, 9-(1,3-Dithiol-2-ylidene)-, and 9-(1,3-Selenathiol-2-ylidene)fluorenes: Synthesis, Intramolecular Charge Transfer, and Redox Properties. *J. Org. Chem.* **1999**, *64*, 6937–6950.
- (47) Mysyk, D. D.; Perepichka, I. F.; Sokolov, N. I. Electron Acceptors of the Fluorene Series. 6. Synthesis of 4,5-Dinitro-9-X-fluorene-2,7-disulfonic Acid Derivatives, Their Charge Transfer Complexes with Anthracene and Sensitization of Photoconductivity of Poly-N-(2,3-epoxypropyl)carbazole. *J. Chem. Soc., Perkin Trans. 2* **1997**, *537*–545.
- (48) Perepichka, D. F.; Bryce, M. R.; Perepichka, I. F.; Lyubchik, S. B.; Christensen, C. A.; Godbert, N.; Batsanov, A. S.; Levillain, E.; McInnes, E. J. L.; Zhao, J. P. A ( $\pi$ -Extended Tetraphiafulvalene)–Fluorene Conjugate. Unusual Electrochemistry and Charge Transfer Properties: The First Observation of a Covalent  $D^{2+}\text{--}\sigma\text{-}A^{\bullet-}$  Redox State. *J. Am. Chem. Soc.* **2002**, *124*, 14227–14238.
- (49) Perepichka, I. F. Electron Acceptors of the Fluorene Series in Photonics and Electronics: Recent Achievements and Perspectives. In *Multiphoton and Light Driven Multielectron Processes in Organics: Materials, Phenomena, Applications*; Kajzar, F.; Agranovich, V. M., Eds.; Book Series NATO Science Series: 3. High Technology; Kluwer Academic Publishers: Dordrecht, The Netherlands, 2000; Vol. 79, pp 371–386.
- (50) Perepichka, I. F.; Kuz'mina, L. G.; Perepichka, D. F.; Bryce, M. R.; Goldenberg, L. M.; Popov, A. F.; Howard, J. A. K. Electron Acceptors of the Fluorene Series. 7. 2,7-Dicyano-4,5-dinitro-9-X-fluorenes: Synthesis, Cyclic Voltammetry, Charge Transfer Complexation with N-Propylcarbazole in Solution, and X-Ray Crystal Structures of Two Tetraphiafulvalene Complexes. *J. Org. Chem.* **1998**, *63*, 6484–6493.
- (51) Perepichka, I. F.; Popov, A. F.; Orekhova, T. V.; Bryce, M. R.; Andrievskii, A. M.; Batsanov, A. S.; Howard, J. A.; Sokolov, N. I. Electron Acceptors of the Fluorene Series. 10. Novel Acceptors Containing Butylsulfanyl, Butylsulfinyl, and Butylsulfonyl Substituents: Synthesis, Cyclic Voltammetry, Charge-Transfer Complexation with

- Anthracene in Solution, and X-Ray Crystal Structures of Two Tetrathiafulvalene Complexes. *J. Org. Chem.* **2000**, *65*, 3053–3063.
- (52) Perepichka, I. F.; Popov, A. F.; Orekhova, T. V.; Bryce, M. R.; Vdovichenko, A. N.; Batsanov, A. S.; Goldenberg, L. M.; Howard, J. A. K.; Sokolov, N. I.; Megson, J. L. Electron Acceptors of the Fluorene Series. Part 5. Intramolecular Charge Transfer in Nitro-substituted 9-(Aminomethylene)fluorenes. *J. Chem. Soc., Perkin Trans. 2* **1996**, 2453–2469.
- (53) Perepichka, D. F.; Perepichka, I. F.; Ivasenko, O.; Moore, A. J.; Bryce, M. R.; Kuz'mina, L. G.; Batsanov, A. S.; Sokolov, N. I. Combining High Electron Affinity and Intramolecular Charge Transfer in 1,3-Dithiole–Nitrofluorene Push-Pull Diads. *Chem.—Eur. J.* **2008**, *14*, 2757–2770.
- (54) Perepichka, D. F.; Perepichka, I. F.; Popov, A. F.; Bryce, M. R.; Batsanov, A. S.; Chesney, A.; Howard, J. A. K.; Sokolov, N. I. Electron Acceptors of the Fluorene Series. Part 12. 9-(Metalloceneylidene)-nitrofluorene Derivatives of Fc-NF, NF–Fc-NF, and NF–Rc-NF Types, and the Vinyllogues Fc–π–NF: Synthesis, Characterisation, Intramolecular Charge Transfer, Redox Properties and X-Ray Structures for Three Fluorene–Ferrocene Derivatives. *J. Organomet. Chem.* **2001**, *637*, 445–462.
- (55) Perepichka, I. F.; Perepichka, D. F.; Lyubchik, S. B.; Bryce, M. R.; Batsanov, A. S.; Howard, J. A. K. Electron Acceptors of the Fluorene Series. Part 13. 9-(5-Nitrofuran-2-ylidene)- and 9-(5-Nitro-2-thienylidene)-2,4,5,7-tetranitrofluorenes: Novel π-Extended Electron Acceptors. Synthesis, Cyclic Voltammetry and X-Ray Crystal Structures for the Acceptor and Its 4,5-Dimethyltetrathiafulvalene Complex, and a Theoretical Study. *J. Chem. Soc., Perkin Trans. 2* **2001**, 1546–1551.
- (56) Batsanov, A. S.; Perepichka, I. F.; Bryce, M. R.; Howard, J. A. K. Cocrystals of 2-(2,4,5,7-Tetranitrofluoren-9-ylidene)propanedinitrile and 2,4,5,7-Tetranitrofluoren-9-one with Chlorobenzene. *Acta Crystallogr., Sect. C* **2001**, *57*, 1299–1302.
- (57) Kuz'mina, L. G.; Perepichka, I. F.; Perepichka, D. F.; Howard, J. A. K.; Bryce, M. R. Supramolecular Architecture of Two Charge-Transfer Complexes Based on 2,7-(X,X)-4,5-Dinitro-9-dicyanomethylenefluorenes (X = NO<sub>2</sub> or CN) and Tetrathiafulvalene. *Crystallogr. Rep.* **2002**, *47*, 251–261.
- (58) Batsanov, A. S.; Bryce, M. R.; Lyubchik, S. B.; Perepichka, I. F. An Unexpected TTFAQ Donor–Fluorene Acceptor Reaction Resulting in a Novel Salt: 2,6-Dihexyloxy-9,10-bis(4,5-dimethyl-1,3-dithiol-2-ylum)-anthracene bis(2,5,7-Trinitro-4-bromo-9-cyanofluorenone) Dioxane Trisolvate. *Acta Crystallogr., Sect. E* **2002**, *58*, 1106–1110.
- (59) Batsanov, A. S.; Perepichka, I. F. 9-Dicyanomethylene-4,5-dinitrofluorene-2,7-disulfonamide. *Acta Crystallogr., Sect. E* **2004**, *60*, 1892–1894.
- (60) Semidetko, O. V.; Chetkina, L. A.; Belskii, V. K.; Mysyk, D. D.; Perepichka, I. F.; Andrievskii, A. M. Some Transformations and Structure of 2,5,7-Trinitro-4-cyanofluorenone, C<sub>14</sub>H<sub>4</sub>N<sub>4</sub>O<sub>7</sub>. *Zh. Obshch. Khim.* **1987**, *57*, 415–420.
- (61) Körzdörfer, T.; Brédas, J.-L. Organic Electronic Materials: Recent Advances in the DFT Description of the Ground and Excited States Using Tuned Range-Separated Hybrid Functionals. *Acc. Chem. Res.* **2014**, *47*, 3284–3291.
- (62) Körzdörfer, T.; Sears, J. S.; Sutton, C.; Brédas, J.-L. Long-Range Corrected Hybrid Functionals for π-Conjugated Systems: Dependence of the Range-Separation Parameter on Conjugation Length. *J. Chem. Phys.* **2011**, *135*, 204107.
- (63) Mori-Sánchez, P.; Cohen, A. J.; Yang, W. Many-Electron Self-Interaction Error in Approximate Density Functionals. *J. Chem. Phys.* **2006**, *125*, 201102.
- (64) Cohen, A. J.; Mori-Sánchez, P.; Yang, W. Insights into Current Limitations of Density Functional Theory. *Science* **2008**, *321*, 792–804.
- (65) Zhao, Y.; Truhlar, D. G. Density Functionals with Broad Applicability in Chemistry. *Acc. Chem. Res.* **2008**, *41*, 157–167.
- (66) Rothberg, L. J.; Yan, M.; Papadimitrakopoulos, F.; Galvin, M. E.; Kwock, E. W.; Miller, T. M. Photophysics of Phenylenevinylene Polymers. *Synth. Met.* **1996**, *80*, 41–58.
- (67) Miyasaka, H.; Kotani, S.; Itaya, A.; Schweitzer, G.; De Schryver, F. C.; Mataga, N. Temperature Effects on the Energy Gap Dependence of Charge Recombination Rates of Ion Pairs Produced by Excitation of Charge-Transfer Complexes Adsorbed on Porous Glass. *J. Phys. Chem. B* **1997**, *101*, 7978–7984.
- (68) Marcus, R. A. On the Theory of Oxidation-Reduction Reactions Involving Electron Transfer. *1. J. Chem. Phys.* **1956**, *24*, 966–978.
- (69) Suppan, P. The Marcus Inverted Region. In *Photoinduced Electron Transfer IV*; Mattay, J., Ed.; Springer: Berlin, 1992; Vol. 163, pp 95–130.
- (70) Kuzmin, M. G.; Soboleva, I. V.; Dolotova, E. V.; Dogadkin, D. N. The Nature of Internal Conversion and Intersystem Crossing in Exciplexes. *High Energy Chem.* **2005**, *39*, 86–96.
- (71) May, V.; Kuhn, O. *Charge and Energy Transfer Dynamics in Molecular Systems*, 3rd ed.; Wiley-VCH: Weinheim, Germany, 2011.
- (72) Englman, R.; Jortner, J. Energy Gap Law for Radiationless Transitions in Large Molecules. *Mol. Phys.* **1970**, *18*, 145–164.
- (73) Bruevich, V. V.; Osotov, M. O.; Paraschuk, D. Yu. Thermal Vibrational Disorder of a Conjugated Polymer in Charge-Transfer Complex. *J. Chem. Phys.* **2009**, *131*, 094906.
- (74) Bakulin, A. A.; Rao, A.; Pavelyev, V. G.; van Loosdrecht, P. H. M.; Pshenichnikov, M. S.; Niedzialek, D.; Cornil, J.; Beljonne, D.; Friend, R. H. The Role of Driving Energy and Delocalized States for Charge Separation in Organic Semiconductors. *Science* **2012**, *335*, 1340–1344.

# Supporting Information

(*J. Phys. Chem. C*, dx.doi.org/10.1021/jp510543c)

## Charge Transfer Dynamics in Donor-Acceptor Complexes between a Conjugated Polymer and Fluorene Acceptors

Vlad G. Pavelyev,<sup>†</sup> Olga D. Parashchuk,<sup>‡</sup> Michal Krompiec,<sup>§,⊥</sup> Tatyana V. Orekhova,<sup>||</sup>  
Igor F. Perepichka,<sup>\*,§</sup> Paul H. M. van Loosdrecht,<sup>†,#</sup> Dmitry Yu. Paraschuk,<sup>‡</sup>  
and Maxim S. Pshenichnikov<sup>\*,†</sup>

<sup>†</sup> Zernike Institute for Advanced Materials, University of Groningen, Nijenborgh 4, 9747 AG Groningen, The Netherlands

<sup>‡</sup> Faculty of Physics and International Laser Center, Lomonosov Moscow State University, Leninskie Gory, 119991 Moscow, Russia

<sup>§</sup> School of Chemistry, Bangor University, Deiniol Road, Bangor LL57 2UW, United Kingdom

<sup>||</sup> L. M. Litvinenko Institute of Physical Organic and Coal Chemistry, National Academy of Sciences of Ukraine, R. Luxemburg Street 70, Donetsk 83114, Ukraine

### Content:

1. Synthesis of fluorene acceptors	p. 2
2. <sup>1</sup> H and <sup>13</sup> C NMR spectra of synthesized fluorene electron acceptors (Figures S1–S16)	p. 7
3. Visible-UV absorption spectra of the acceptors (Figure S17)	p. 23
4. DFT B3LYP/6-31+G(d) calculations (Tables S1, S2; Figures S18–S20)	p. 24
5. Ultrafast spectroscopy data (Table S3)	p. 29
6. References	p. 30

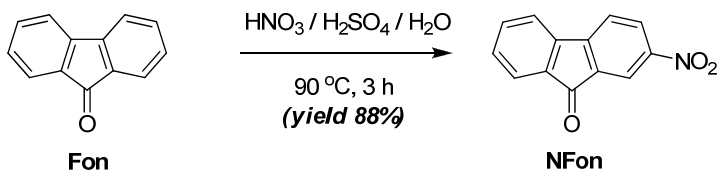
\* Corresponding Authors. E-mails: M.S.Pshenichnikov@rug.nl; i.perepichka@bangor.ac.uk

† Present address: Merck Chemicals Ltd., Chilworth Technical Centre, University Parkway, Southampton, SO16 7QD, U.K.

# Present address: II. Physikalisches Institut, Universität zu Köln, 50923 Köln, Germany.

## **1. Synthesis of fluorene acceptors**

### **2-Nitro-9-fluorenone (NFon).**



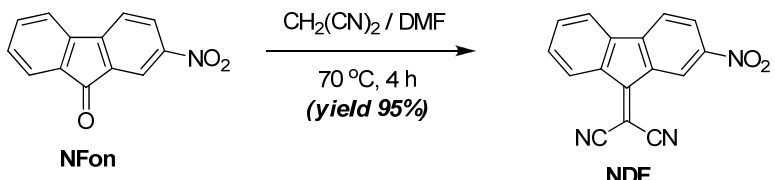
A mixture of 9-fluorenone (**Fon**) (10.0 g, 55.5 mmol),  $\text{HNO}_3$  (71%, d = 1.41 g mL<sup>-1</sup>; 10.0 mL, 160 mmol),  $\text{H}_2\text{SO}_4$  (96%, d = 1.84 g mL<sup>-1</sup>; 10.0 mL, 195 mmol) and water (10.0 mL) were stirred with heating at 90 °C for 3 hours. After cooling to room temperature, mixture was poured into water (250 mL), precipitate was filtered off, washed several times with water until pH = 7 and dried. Crude product was recrystallized from ethanol to afford compound **NFon** (11.0 g, 88.0%) as light yellow needles, mp 222–224 °C. Repeated recrystallization from ethanol gave compound **NFon** with mp 223.5–224 °C.

Lit. mp 222–223 °C.<sup>1</sup>

<sup>1</sup>H NMR (400 MHz,  $\text{CDCl}_3$ ):  $\delta$  8.47 (d, J = 2.0 Hz, 1H), 8.42 (dd, J = 8.2 Hz, J = 2.1 Hz, 1H), 7.77 (d, J = 7.4 Hz, 1H), 7.72–7.66 (m, 2H), 7.61 (td, J = 7.5 Hz, J = 0.9 Hz, 1H), 7.46 (td, J = 7.4 Hz, J = 0.8 Hz, 1H).

<sup>13</sup>C NMR (100 MHz,  $\text{CDCl}_3$ ): 190.94 (C=O), 149.74, 148.78, 142.32, 135.45, 135.06, 135.01, 131.02, 129.94, 125.11, 121.80, 120.71, 119.56.

### **2-Nitro-9-dicyanomethylenefluorene (NDF).**



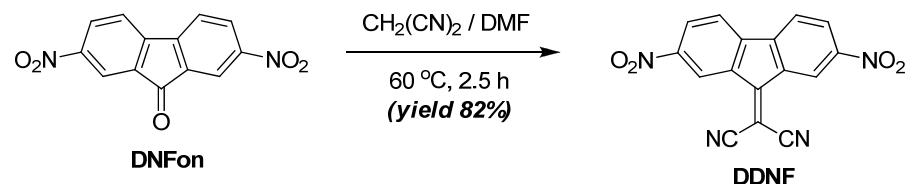
2-Nitrofluorenone (10.0g, 44.4 mmol) was suspended in *N,N*-dimethylformamide (DMF) (100 mL) at ca. 60–70 °C. Malononitrile (9.30 g, 141 mmol, 3.2 eq.) was added and the mixture was stirred at 70 °C for 4 hours and left to stay overnight at room temperature. The precipitate was filtered off, washed with DMF, then with ethanol and dried to afford compound **NDF** (11.50 g, 94.8%) as orange crystals, mp 272–274 °C.

<sup>1</sup>H NMR (400 MHz,  $\text{CDCl}_3$ ):  $\delta$  9.28 (d, 1H, J = 1.8 Hz, H-1), 8.51 (d, 1H, J = 8.0 Hz), 8.44 (dd, 1H, J = 8.2 Hz, J = 1.9 Hz), 7.76 (d, 1H, J = 8.3 Hz), 7.73 (d, 1H, J = 7.6 Hz), 7.64 (dd, 1H, J = 7.7 Hz, J = 7.7 Hz), 7.51 (dd, 1H, J = 7.5 Hz, J = 7.5 Hz).

<sup>1</sup>H NMR (400 MHz,  $\text{DMSO-d}_6$  + a drop of  $\text{CF}_3\text{CO}_2\text{H}^*$ ):  $\delta$  9.31 (d, 1H, J = 1.9 Hz, H-1), 8.54 (dd, 1H, J = 8.4 Hz, J = 2.0 Hz), 8.34 (d, 1H, J = 7.9 Hz, 8.20 (d, 1H, J = 8.4 Hz), 8.13 (bd, 1H, J = 7.5 Hz), 7.76 (ddd, 1H, J = 7.5 Hz, J = 7.5 Hz, J = 0.7 Hz), 7.64 (ddd, 1H, J = 7.7 Hz, J = 7.7 Hz, J = 0.9 Hz).

*\* a drop of an acid was added to get a well resolved NMR spectrum; as it was shown previously, pronounced broadening of aromatic signals with loss of fine spin-spin splitting (br.s. or even disappearing the proton signals) is observed for strong electron acceptors of the fluorene series in polar solvents (DMSO, DMF, acetone), due to paramagnetic broadening effect.<sup>2,3</sup>*

## 2,7-Dinitro-9-dicyanomethylenefluorene (DDNF).



2,7-Dinitrofluorenone (8.00g, 29.6 mmol) was dissolved in DMF (80 mL) at ca. 80 °C. Malononitrile (5.00 g, 75.7 mmol, 2.56 eq.) was added, the mixture was stirred at 60–70 °C for 2.5 hours (starting compound is dissolved in ca. 10 min and the product starts to crystallize in ca. 30 min) and left to stay overnight at room temperature for crystallization. The precipitate was filtered off, washed with DMF (10 mL), then with ethanol and dried to afford compound **DDNF** (7.78 g, 82.6%) as bright yellow crystals, mp 311–312 °C.

Lit. mp 298–299 °C.<sup>4</sup>

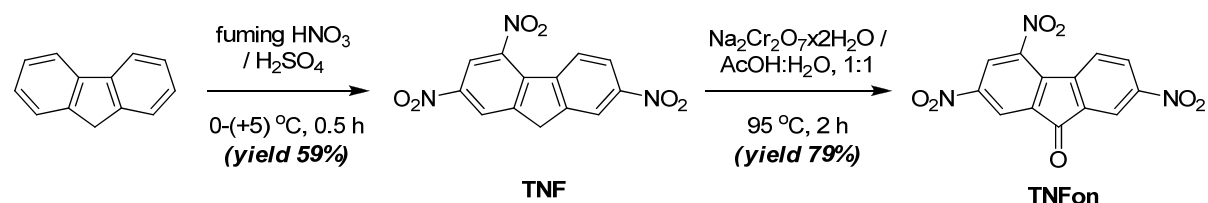
<sup>1</sup>H NMR (400 MHz, CDCl<sub>3</sub>): δ 9.38 (2H, d, J = 1.8 Hz, H-1,8), 8.55 (2H, dd, J = 8.3 Hz, J = 1.8 Hz, H-3,6), 7.94 (2H, d, J = 8.3 Hz, H-4,5).

<sup>1</sup>H NMR (400 MHz, DMSO-d<sub>6</sub> + a drop of CF<sub>3</sub>CO<sub>2</sub>H<sup>\*</sup>): δ 9.08 (2H, d, J = 1.6 Hz), 8.63 (2H, dd, J = 8.3 Hz, J = 1.2 Hz), 8.42 (2H, d, J = 8.3 Hz).

<sup>13</sup>C NMR (100 MHz, DMSO-d<sub>6</sub> + a drop of CF<sub>3</sub>COOH): δ: 156.30, 149.22, 145.15, 135.72, 130.74, 124.64, 121.26, 113.19, 81.50.

\*<sup>a</sup> a drop of an acid was added to get a well resolved NMR spectrum; as it was shown previously, large broadening of aromatic signals with loss of fine spin-spin splitting (br.s. or even disappearing the proton signals) is observed for strong electron acceptors of the fluorene series in polar solvents (DMSO, DMF, acetone), due to paramagnetic broadening effect.<sup>2,3</sup>

## 2,4,7-Trinitro-9-fluorenone (TNFon).

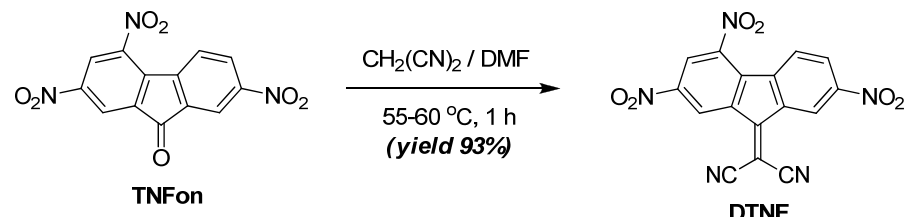


A) **2,4,7-Trinitrofluorene (TNF)** was obtained by nitration of fluorene with a mixture of fuming nitric acid and concentrated sulphuric acid at 0–5 °C for 30 min, as described previously,<sup>5</sup> mp 210–211 °C.

B) **2,4,7-Trinitro-9-fluorenone (TNFon).** 2,4,7-Trinitrofluorene (**TNF**) (9.04 g, 30.0 mmol) in 50% aqueous acetic acid (200 mL) was heated with stirring on a steam bath to 95 °C. Na<sub>2</sub>Cr<sub>2</sub>O<sub>7</sub>·2H<sub>2</sub>O (12.5 g, 42 mmol) was added by portions for ca. 15 min keeping the temperature around 95 °C. The mixture was stirred at this temperature for 2 hour, cooled down to room temperature and poured into ice water (300 mL). Yellow precipitate was filtered off, washed with diluted aqueous HCl for removal chromium salt, then with water until pH = 7 and dried to afford **TNFon** (9.10 g, 96.3%), mp 167–172 °C. Crude product was recrystallized from acetic acid (ca. 45 mL) to afford pure **TNFon** (7.45 g, 78.8%) as yellow needles, mp 175–176 °C. Lit. mp 175–176 °C.<sup>6,7</sup>

<sup>1</sup>H NMR (400 MHz, CDCl<sub>3</sub>): δ 9.04 (d, 1H, J = 2.1 Hz, H-3), 8.83 (d, 1H, J = 2.1 Hz, H-1), 8.68 (d, 1H, J = 2.2 Hz, H-8), 8.58 (dd, 1H, J = 8.6 Hz, J = 2.3 Hz, H-6), 8.38 (d, 1H, J = 8.6 Hz, H-5).  
<sup>13</sup>C NMR (100 MHz, CDCl<sub>3</sub>, DEPTQ): δ 185.97 (C=O), 150.30, 149.23, 145.13, 143.37, 139.50, 138.42, 136.31, 130.79, 128.22, 125.87, 123.03, 120.21.

**2,4,7-trinitro-9-dicyanomethylenefluorene (DTNF)** was obtained according to our modified procedure described for condensation of other polynitrofluorenones with malononitrile in DMF.<sup>2,3,8,9,10</sup>



2,4,7-Trinitrofluorenone, **TNFon** (10.00 g, 31.7 mmol) was dissolved in DMF (50 mL) with heating to ca. 55 °C and malononitrile (4.60 g, 69.6 mmol, 2.2 eq.) was added in one portion. The reaction mixture was stirred at 55–60 °C for 1 hour, diluted with propan-2-ol (200 mL) and left to crystallize in a fridge (+5 °C, 4h). Yellow solid was filtered off, washed with ethanol and dried to afford **DTNF** (10.75g, 93.3 %). It can be recrystallized from acetonitrile or dioxane to yield pure **DTNF** as bright yellow crystals, mp 267–268 °C.

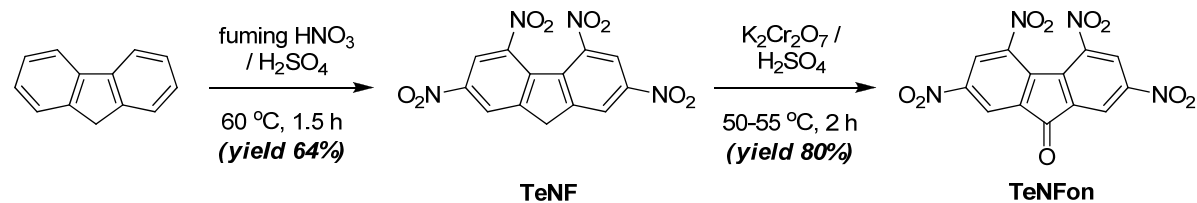
Lit. m.p. 266–268 °C.<sup>11</sup>

<sup>1</sup>H NMR (400 MHz, acetone-d<sub>6</sub>): δ 9.9–8.9 (m, 3H), 9.37 (m, 2H).\*)

<sup>1</sup>H NMR (400 MHz, CDCl<sub>3</sub>): δ 9.69 (d, 1H, J = 1.0 Hz, H-1), 9.51 (d, 1H, J = 1.0 Hz, H-8), 8.95 (bs, 1H, H-3), 8.58 (dd, 1H, J = 8.6 Hz, J = 1.5 Hz, H-6), 8.24 (d, 1H, J = 8.8 Hz, H-5).

\*<sup>1</sup> Paramagnetic broadening of aromatic protons in acetone,<sup>2,3</sup> similar to that observed for **DDNF** and **DTeNF**.

### 2,4,5,7-Tetranitro-9-fluorenone (TeNFon).



**A) 2,4,5,7-Tetranitrofluorene (TeNF)** was obtained by nitration of fluorene with a mixture of fuming nitric acid and concentrated sulphuric acid at 60 °C for 1.5 hours, as described previously,<sup>5</sup> mp 278–280 °C (decomp).

**B) 2,4,5,7-Tetranitro-9-fluorenone (TeNFon).** 2,4,5,7-Tetranitrofluorene (**TeNF**) (16.1g, 46.5 mmol) was suspended in concentrated H<sub>2</sub>SO<sub>4</sub> (96%; 100 mL) and with stirring K<sub>2</sub>Cr<sub>2</sub>O<sub>7</sub> (24.1g, 82 mmol) was added by portions for ca. 30 min, keeping temperature around 50 °C. The mixture was stirred at 50–55 °C for 2 hours, cooled down to room temperature and poured into ice-water (1 L). Yellow precipitate was filtered off, washed with diluted H<sub>2</sub>SO<sub>4</sub> (20%; 2×50 mL), then with water until pH = 7 and dried to

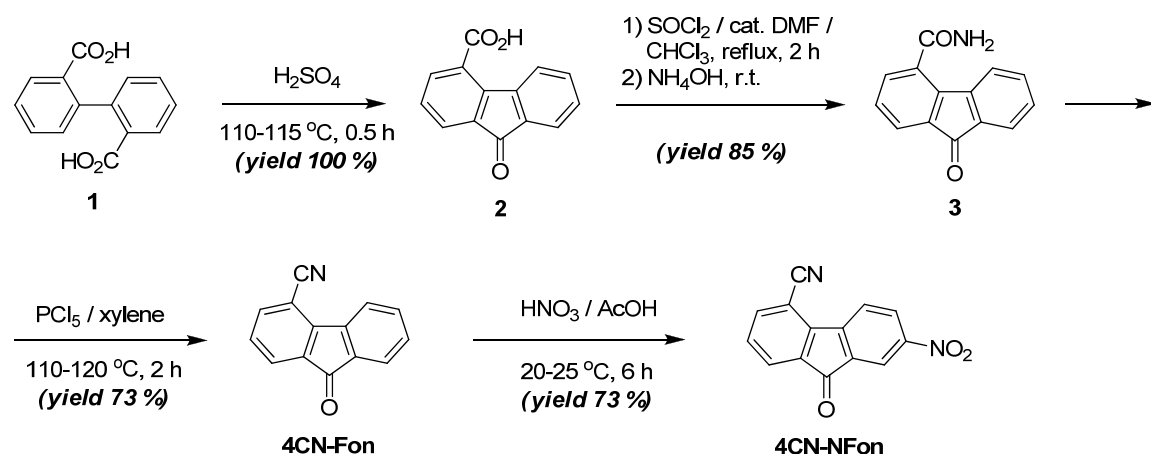
afford crude product **TeNFon** (16.0 g, 95.5%), mp 241–245 °C. Crude compound was dissolved under reflux in dioxane (ca. 30 mL) and left to crystallize at +12 °C. Precipitated crystals were filtered off, washed on filter with 2 mL of cold dioxane and dried under *vacuo* at +100 °C, affording pure **TeNFon** (13.4 g, 80.0%) as light-yellow crystals, mp 251–252 °C (**TeNFon** forms crystallosolvate with dioxane, which loose dioxane at elevated temperature).

Lit. mp 252–253 °C.<sup>12</sup>

<sup>1</sup>H NMR (400 MHz, CDCl<sub>3</sub>): δ 9.05 (2H, d, J = 1.9 Hz, H-3,6), 8.91 (2H, d, J = 1.9 Hz, H-1,8).

<sup>13</sup>C NMR (100 MHz, CDCl<sub>3</sub>): δ 183.50 (C=O), 150.09, 146.83, 138.63, 137.51, 125.72, 123.03.

### 2-Nitro-5-cyanofluorenone (4CN-NFon).



**A) 9-Fluorenone-4-carboxylic acid (2).** Diphenic acid (**1**) (40.0g, 165 mmol) and H<sub>2</sub>SO<sub>4</sub> (96%; d = 1.84 g mL<sup>-1</sup>; 80 mL) were stirred with heating at 110–115 °C for 30 min (in 5–10 min, diphenic acid is dissolved to give deep red solution). The mixture was cooled down to room temperature and poured into ice-water (400 mL). Yellow precipitate was filtered off, thoroughly washed with water until pH = 7 and dried to afford acid **2** (36.85 g, 99.5%), mp 222–224 °C. The product is pure enough; recrystallization from acetic acid (300 mL) afforded compound **2** (33.05g, 89.3%) as yellow needles, mp 225.5–226.5 °C.

Lit. mp 220–221 °C,<sup>13</sup> 226 °C.<sup>14</sup>

<sup>1</sup>H NMR (400 MHz, DMSO-d<sub>6</sub>): δ 13.68 (1H, bs, COOH), 8.25 (1H, bd, J = 7.7 Hz), 7.97–7.93 (1H, m), 7.82–7.76 (1H, m), 7.69–7.59 (2H, m), 7.51–7.40 (2H, m).

<sup>13</sup>C NMR (100 MHz, DMSO-d<sub>6</sub>): δ 192.66, 168.46, 143.06, 142.67, 136.51, 135.91, 135.00, 134.09, 130.49, 129.82, 128.73, 127.05, 126.18, 124.30.

**B) 9-Fluorenone-4-carboxamide (3).** 9-Fluorenone-4-carboxylic acid (**2**) (12.35 g, 55.1 mmol), SO<sub>2</sub>Cl<sub>2</sub> (7.0 g, 65 mmol) and catalytic amount of DMF (3 drops) in chloroform (30 mL) were been refluxed with stirring for 2 hours (full dissolution in 10–15 min). After cooling to room temperature, mixture was poured in vigorously stirred ammonia (25% aqueous solution, 100 mL). Yellow precipitate was filtered off, washed with 10% aqueous ammonia, then with water until pH = 7 and dried to afford compound **3** (10.42 g, 84.7%), mp 229–230 °C. The product is pure enough; after recrystallization from DMF (5–7 mL DMF per 1 g of compound **3**), mp 230–231 °C.

Lit. mp 223–224 °C,<sup>13</sup> 230–230.5 °C.<sup>15</sup>

<sup>1</sup>H NMR (400 MHz, DMSO-d<sub>6</sub> + a drop of CF<sub>3</sub>CO<sub>2</sub>H): δ 8.22 (1H, bs, NH), 7.88 (1H, d, 7.0 Hz), 7.81 (1H, bs, NH), 7.72–7.58 (4H, m), 7.47–7.38 (2H, m).

<sup>13</sup>C NMR (100 MHz, DMSO-d<sub>6</sub> + a drop of CF<sub>3</sub>CO<sub>2</sub>H): δ 192.95, 169.98, 143.31, 140.35, 135.85, 134.32, 134.25, 133.85, 133.53, 130.13, 129.76, 125.05, 124.52, 124.35.

**C) 4-Cyano-9-fluorenone (4CN-Fon).**<sup>16</sup> To a suspension of 9-fluorenone-4-carboxamide (**3**) (30.0 g, 134 mmol) in xylene (200 mL), PCl<sub>5</sub> (33.0 g, 158 mmol) was added and mixture was heated with stirring at 110–120 °C for 2 hours. The solvent was evaporated under reduced pressure, water (400 mL) was added to the residue and mixture was neutralized by adding saturated Na<sub>2</sub>CO<sub>3</sub> solution. Precipitate was filtered off, suspended in hot water (400 mL), filtered again, washed with water (3×150 mL) and dried to afford product **4CN-Fon** (26.1 g, 94.6%). Crude product was recrystallized from dioxane to give pure compound **4CN-Fon** (20.1 g, 72.9%) as bright yellow needles, mp 241–242 °C.

Lit. mp 240–241 °C,<sup>16</sup> 238–240 °C.<sup>17</sup>

<sup>1</sup>H NMR (400 MHz, CDCl<sub>3</sub>): δ 8.22 (1H, d, J = 7.6 Hz), 7.87 (1H, dd, J = 7.4 Hz, J = 0.9 Hz), 7.75 (1H, broad d, J = 7.4 Hz), 7.71 (1H, dd, J = 7.8 Hz, J = 0.9 Hz), 7.62 (1H, ddd, J = 7.6 Hz, J = 7.6 Hz, J = 1.0 Hz), 7.45 (1H, broad dd, J = 7.5 Hz, J = 7.5 Hz), 7.42 (1H, dd, J = 7.6 Hz, J = 7.6 Hz).

<sup>13</sup>C NMR (100 MHz, CDCl<sub>3</sub>): δ 191.23 (C=O), 146.37, 141.59, 137.51, 135.56, 134.86, 133.83, 130.91, 129.41, 127.97, 124.83, 122.76, 117.06, 105.36.

**D) 2-Nitro-5-cyano-9-fluorenone (4CN-NFon).**<sup>18</sup> 4-Cyano-9-fluorenone (2.15 g, 10.5 mmol) was added by portions to the mixture of fuming nitric acid (d = 1.50 g mL<sup>-1</sup>, 20 mL) and acetic acid (10 mL), with stirring. The mixture was stirred at room temperature for 6 hours (crystallization of the product starts in ca. 20–30 min) and poured into ice-water (150 mL). Precipitate was filtered off, washed with water until pH = 7 and dried to afford crude product **4CN-NFon** (2.39 g, 91.2%), mp 227–230 °C. Recrystallization from toluene (~20 mL) yielded pure compound **4CN-NFon** (1.92g, 73.2%) as light yellow crystals, mp 231–232.5 °C.

Lit. mp 230–231 °C.<sup>18</sup>

<sup>1</sup>H NMR (400 MHz, CDCl<sub>3</sub>): δ 8.56 (1H, d, J = 2.03 Hz), 8.53 (1H, dd, J = 8.3 Hz, J = 2.2 Hz), 8.44 (1H, d, J = 8.3 Hz), 8.01 (1H, dd, J = 7.5 Hz, J = 0.9 Hz), 7.86 (1H, dd, J = 7.8 Hz, J = 0.9 Hz), 7.60 (1H, dd, J = 7.6 Hz, J = 7.6 Hz).

<sup>13</sup>C NMR (100 MHz, CDCl<sub>3</sub>): δ 188.52 (C=O), 175.07, 149.65, 146.47, 144.05, 138.28, 135.56, 134.87, 131.26, 130.50, 128.70, 123.29, 119.87, 116.46, 106.85.

## **2. $^1\text{H}$ and $^{13}\text{C}$ NMR spectra of synthesized fluorene electron acceptors**

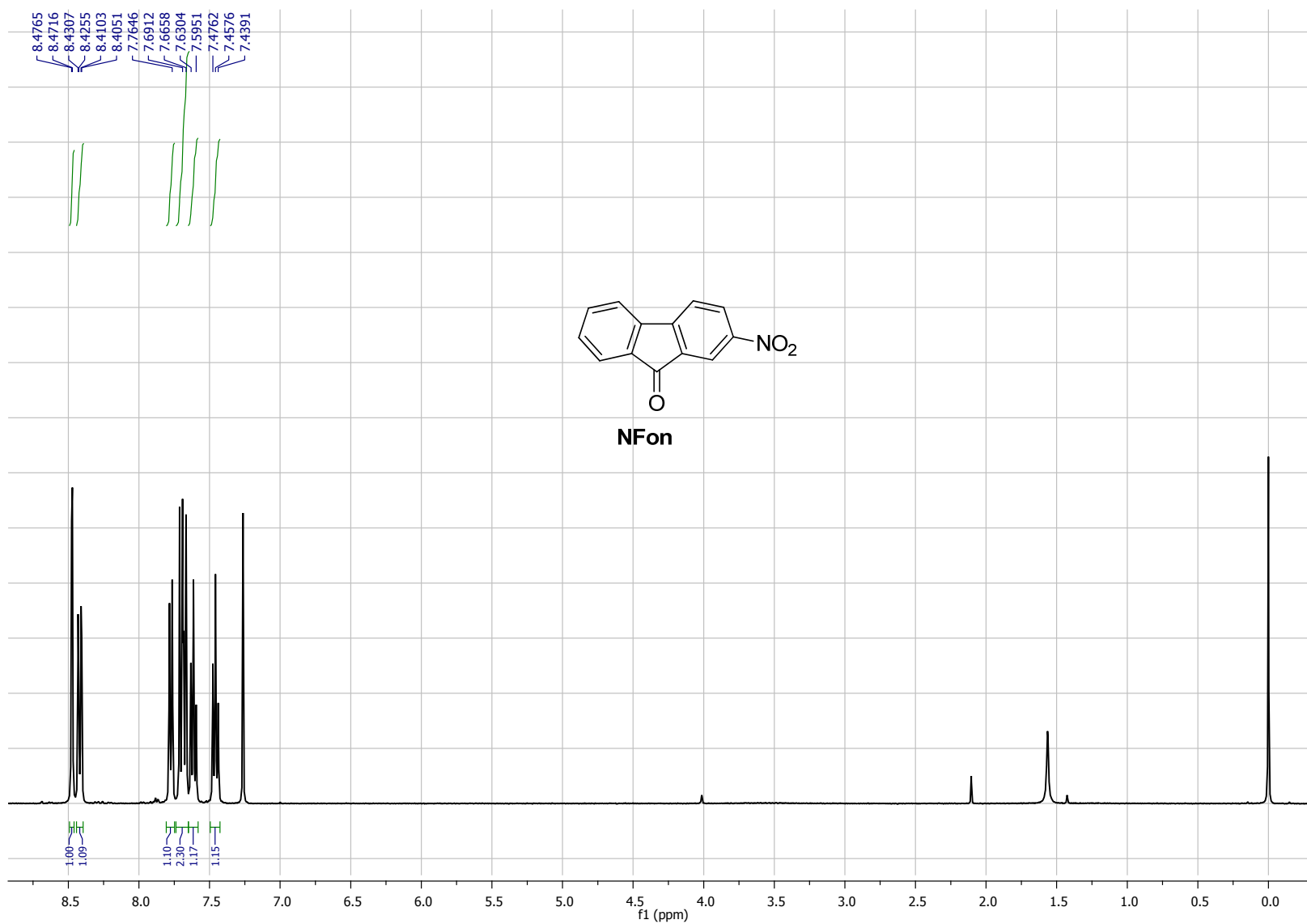


**Figure S1.**  $^1\text{H}$  NMR spectrum of 2-nitro-9-fluorenone (Nfon) in chloroform- $d$ .

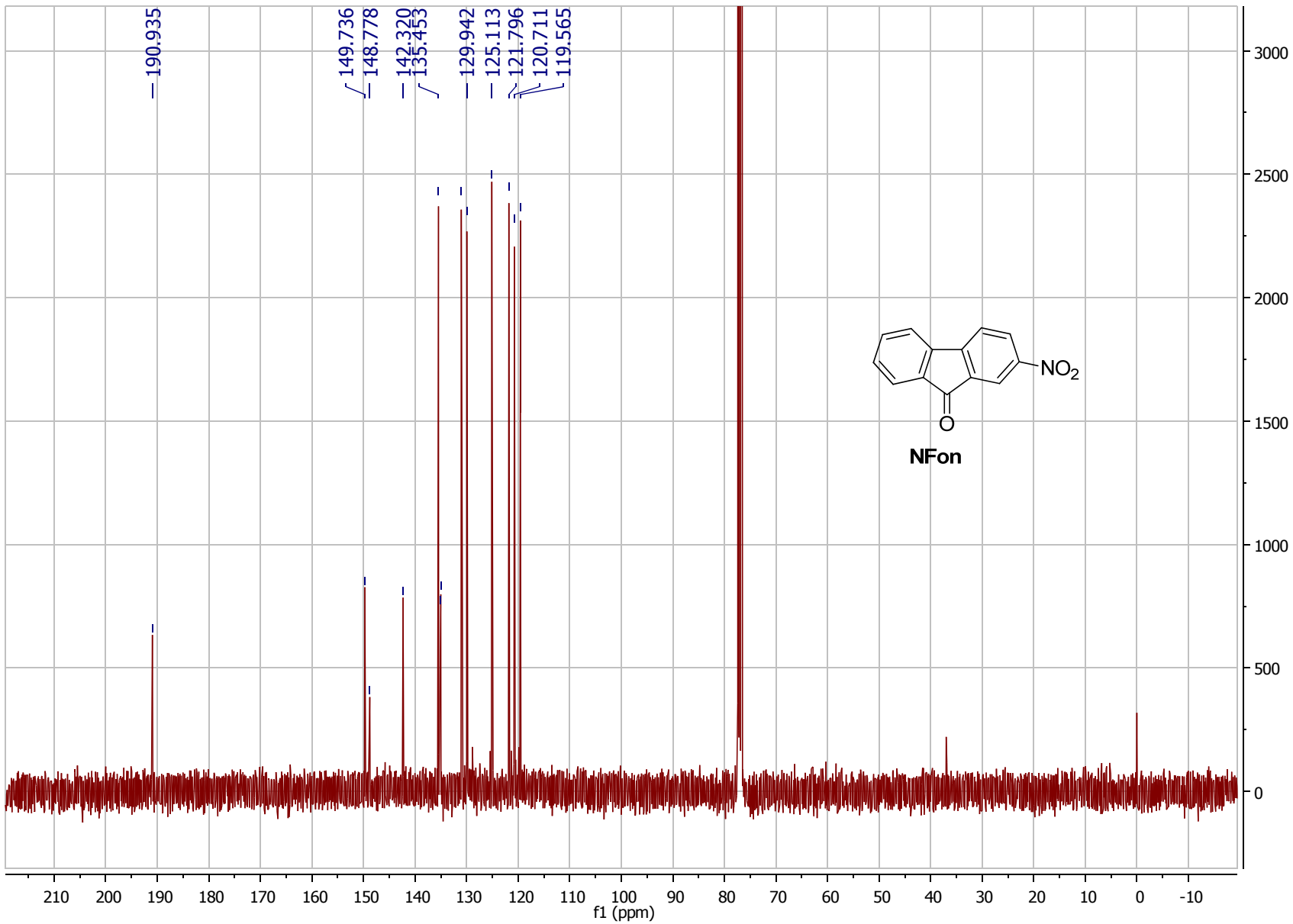


**Figure S2.**  $^{13}\text{C}$  NMR spectrum of 2-nitro-9-fluorenone (**NFlon**) in chloroform-*d*.

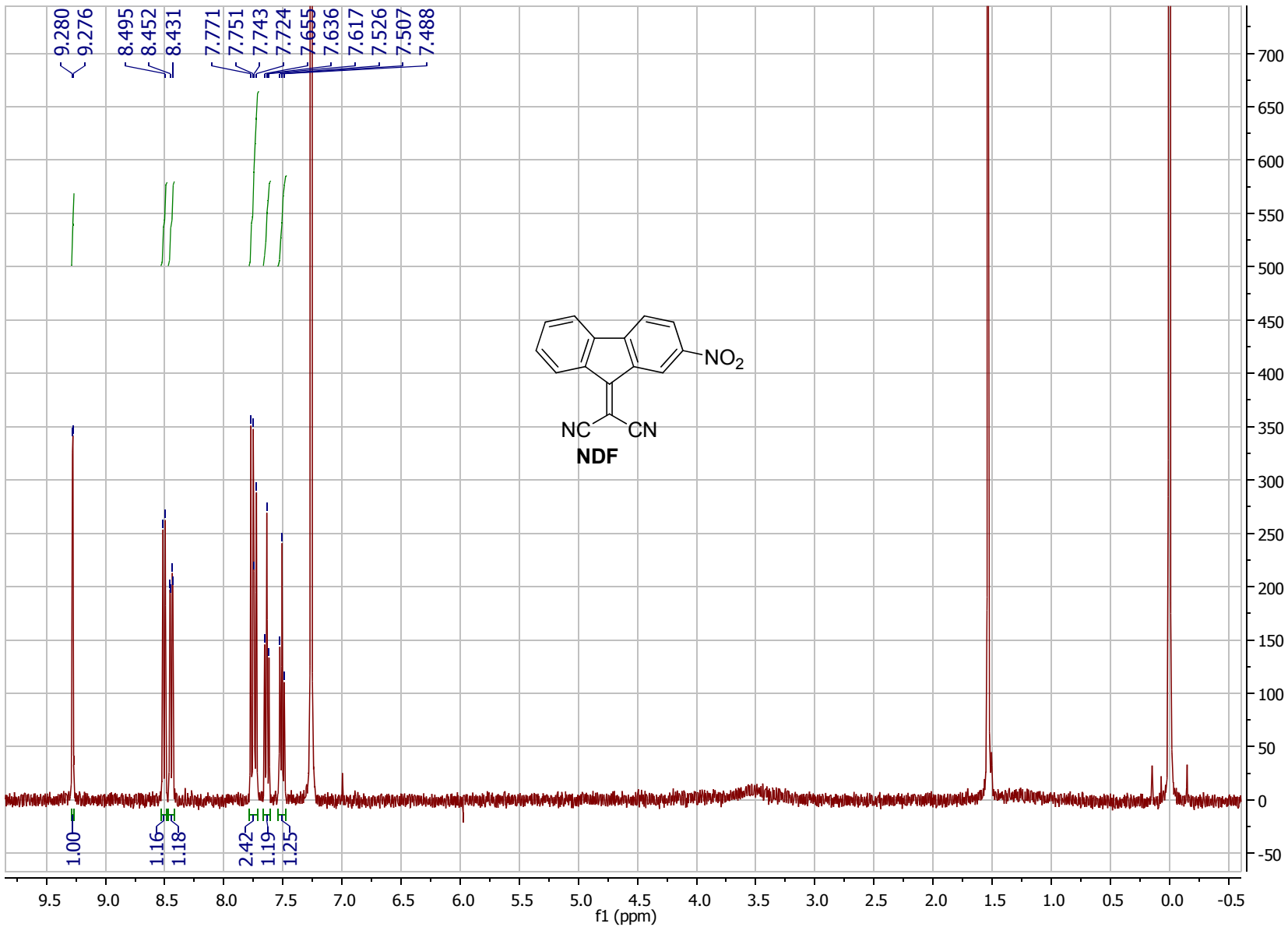


**Figure S3.**  $^1\text{H}$  NMR spectrum of 2-nitro-9-dicyanomethylenefluorene (**NDF**) in chloroform- $d$ .

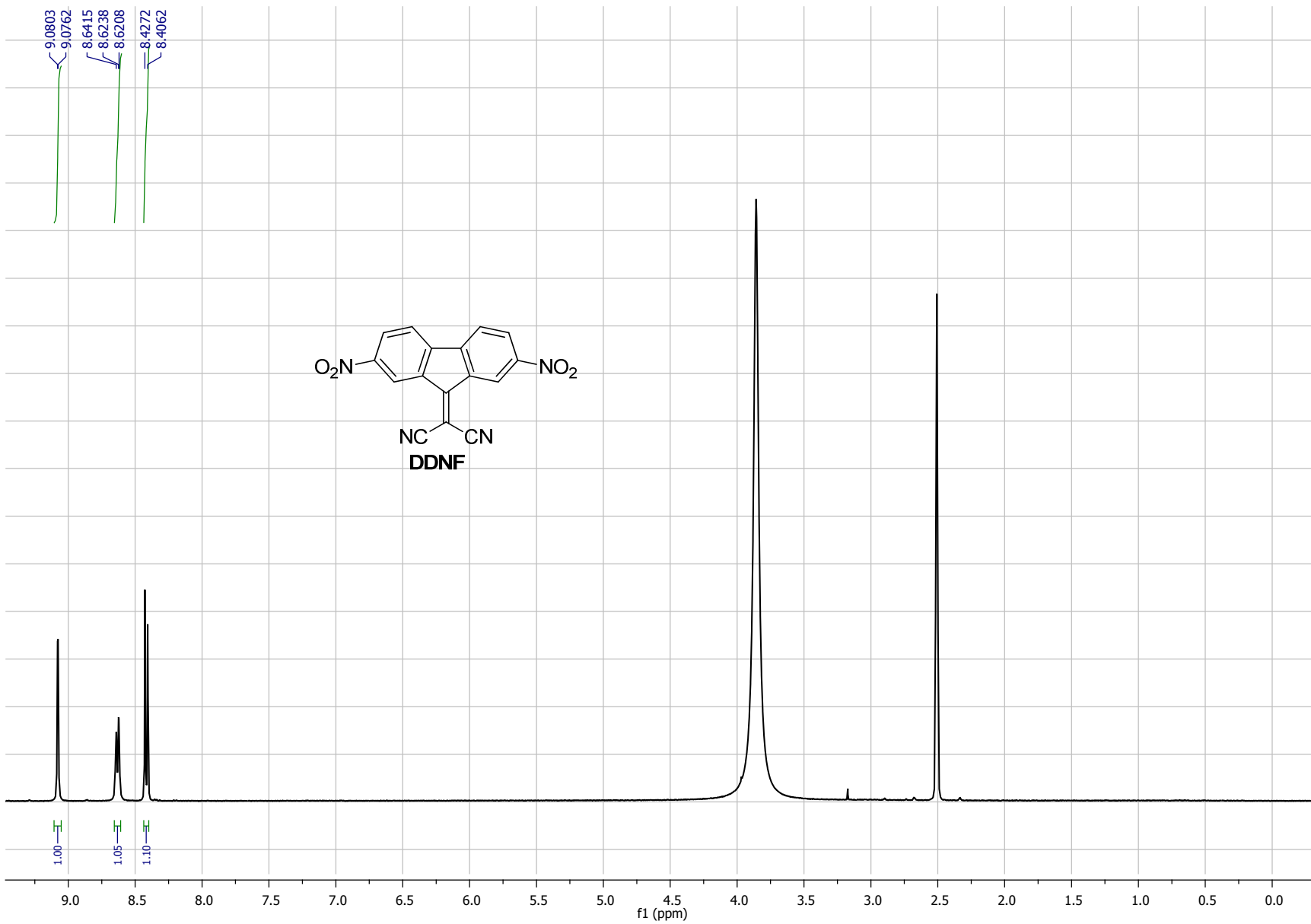


**Figure S4.**  $^1\text{H}$  NMR spectrum of 2,7-dinitro-9-dicyanomethylenefluorene (**DDNF**) in ( $\text{DMSO}-d_6 + \text{a drop of } \text{CF}_3\text{COOH}$ ).

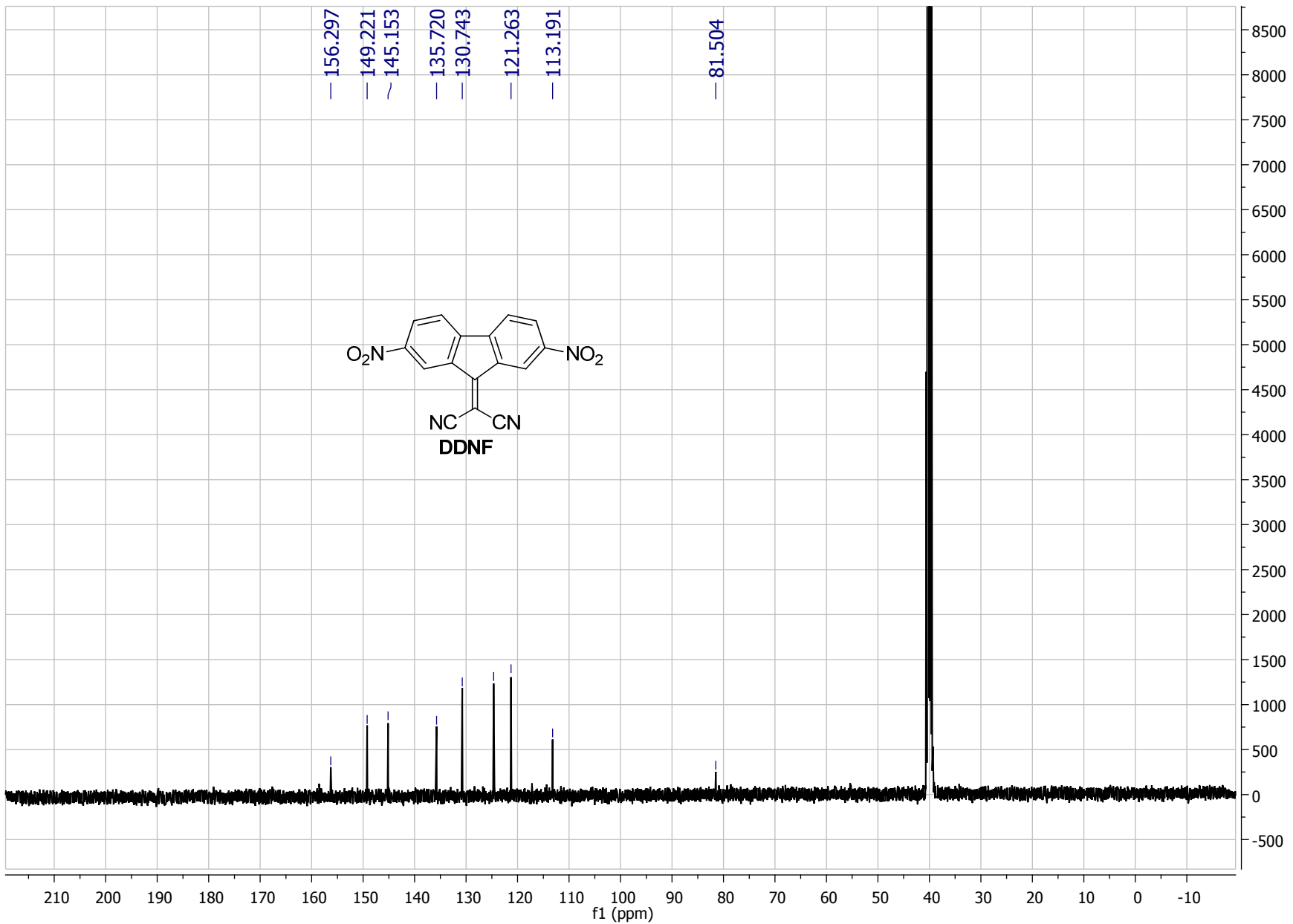


**Figure S5.**  $^{13}\text{C}$  NMR spectrum of 2,7-dinitro-9-dicyanomethylenefluorene (**DDNF**) in (DMSO- $d_6$  + a drop of  $\text{CF}_3\text{COOH}$ ).

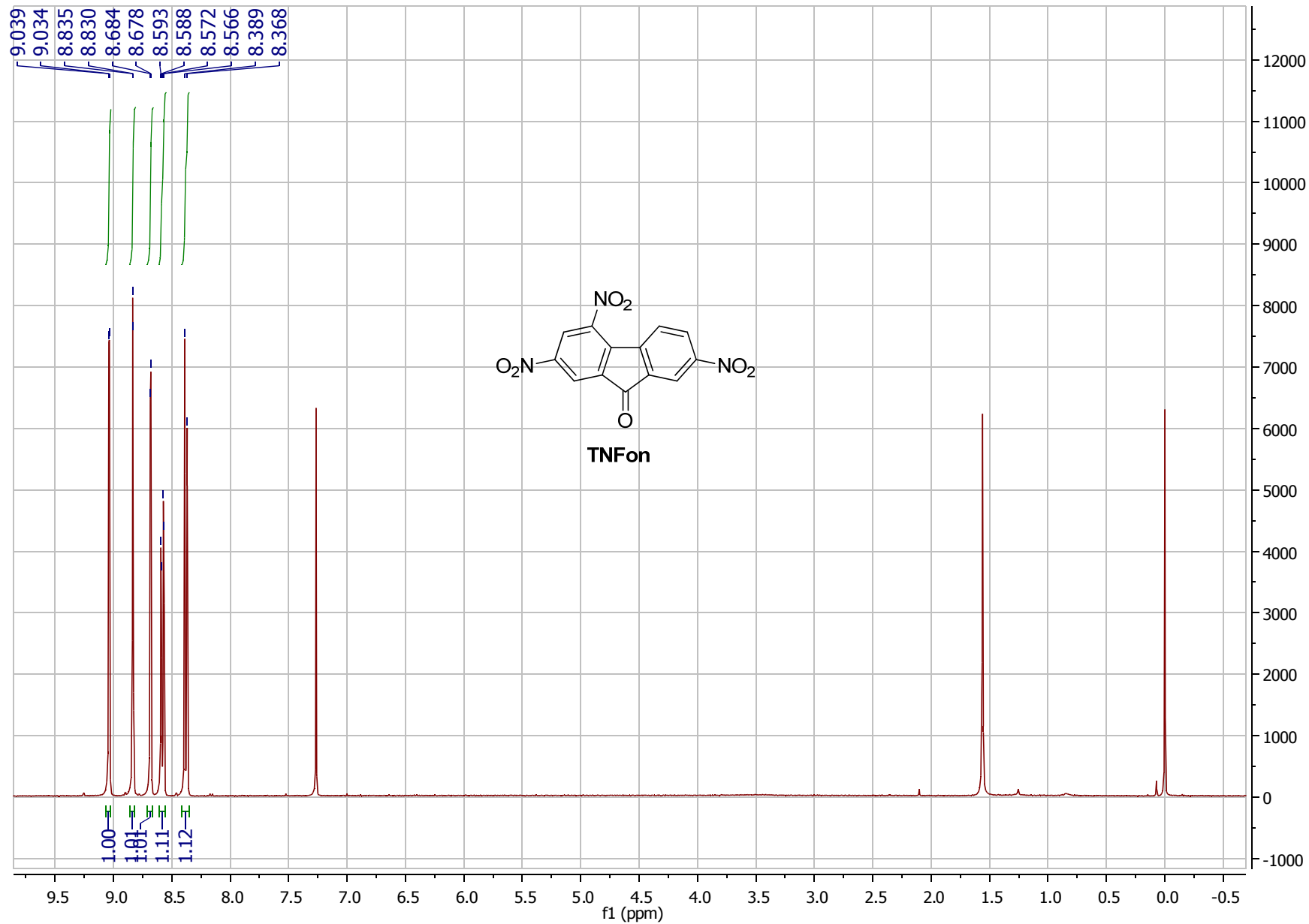


**Figure S6.**  $^1\text{H}$  NMR spectrum of 2,4,7-trinitro-9-fluorenone (TNFon) in chloroform- $d$ .

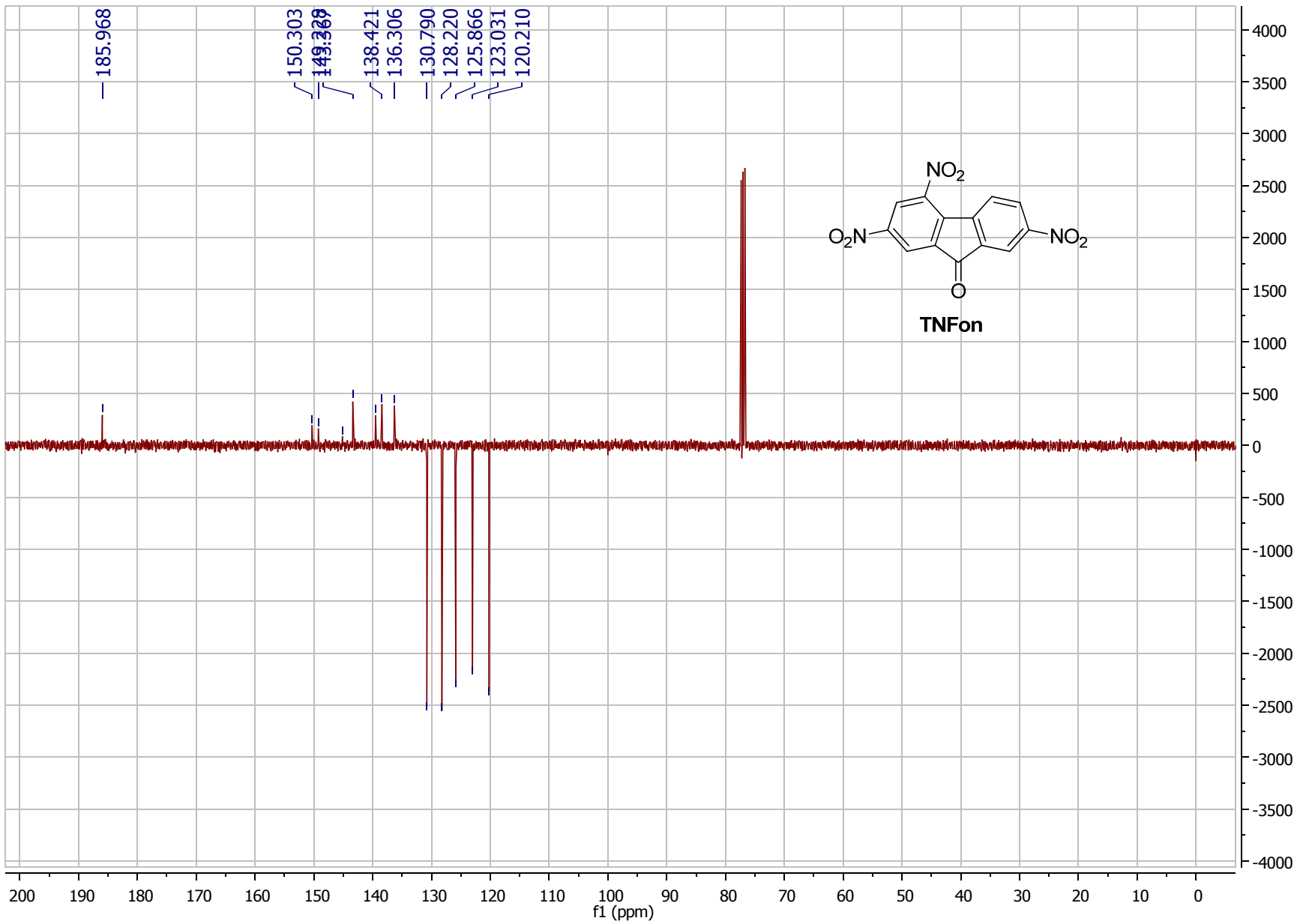


**Figure S7.**  $^{13}\text{C}$  NMR (DEPTQ) spectrum of 2,4,7-trinitro-9-fluorenone (**TNFon**) in chloroform-*d*.

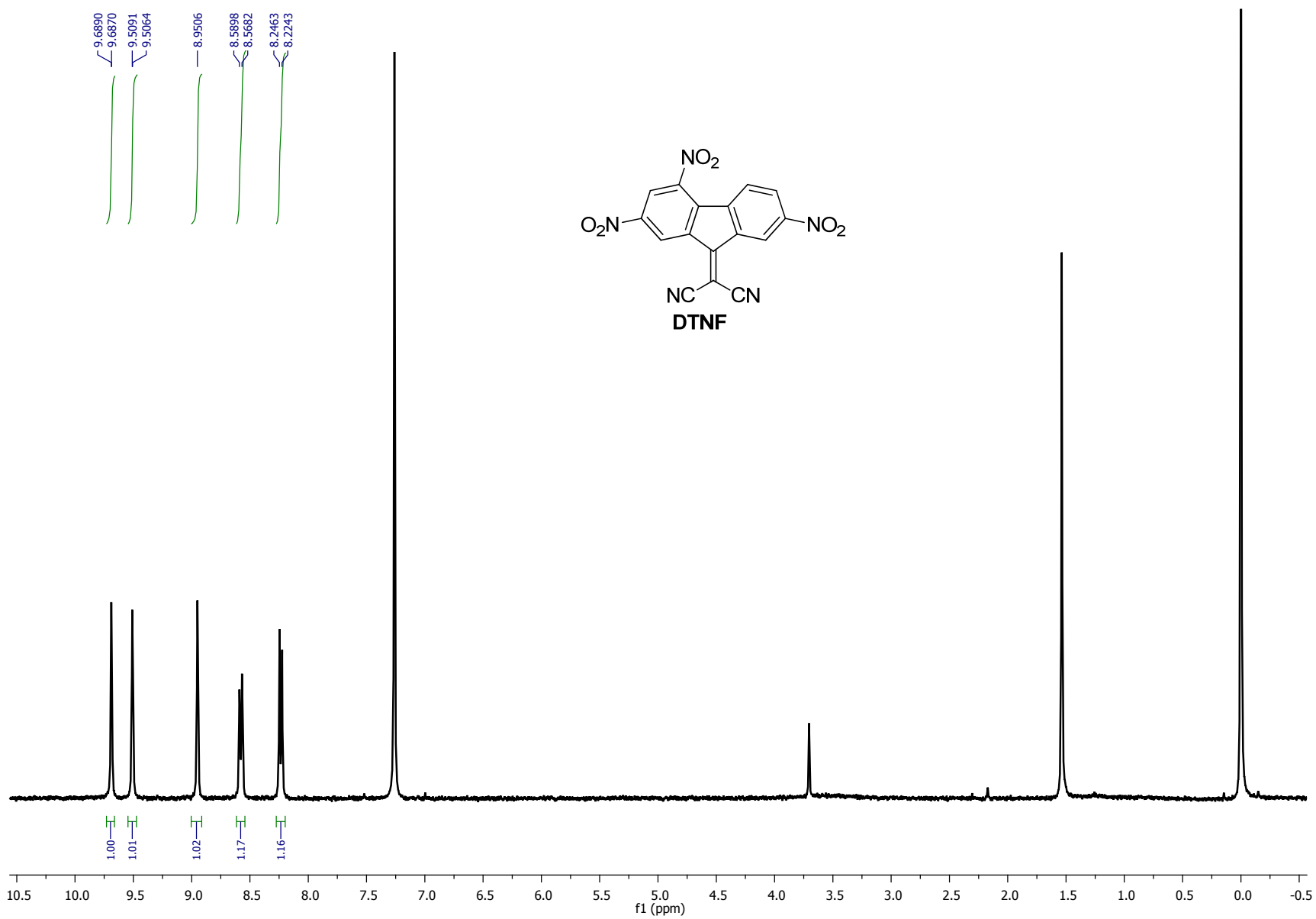


**Figure S8.**  $^1\text{H}$  NMR spectrum of 2,4,7-trinitro-9-dicyanomethylenefluorene (**DTNF**) in chloroform-*d*.

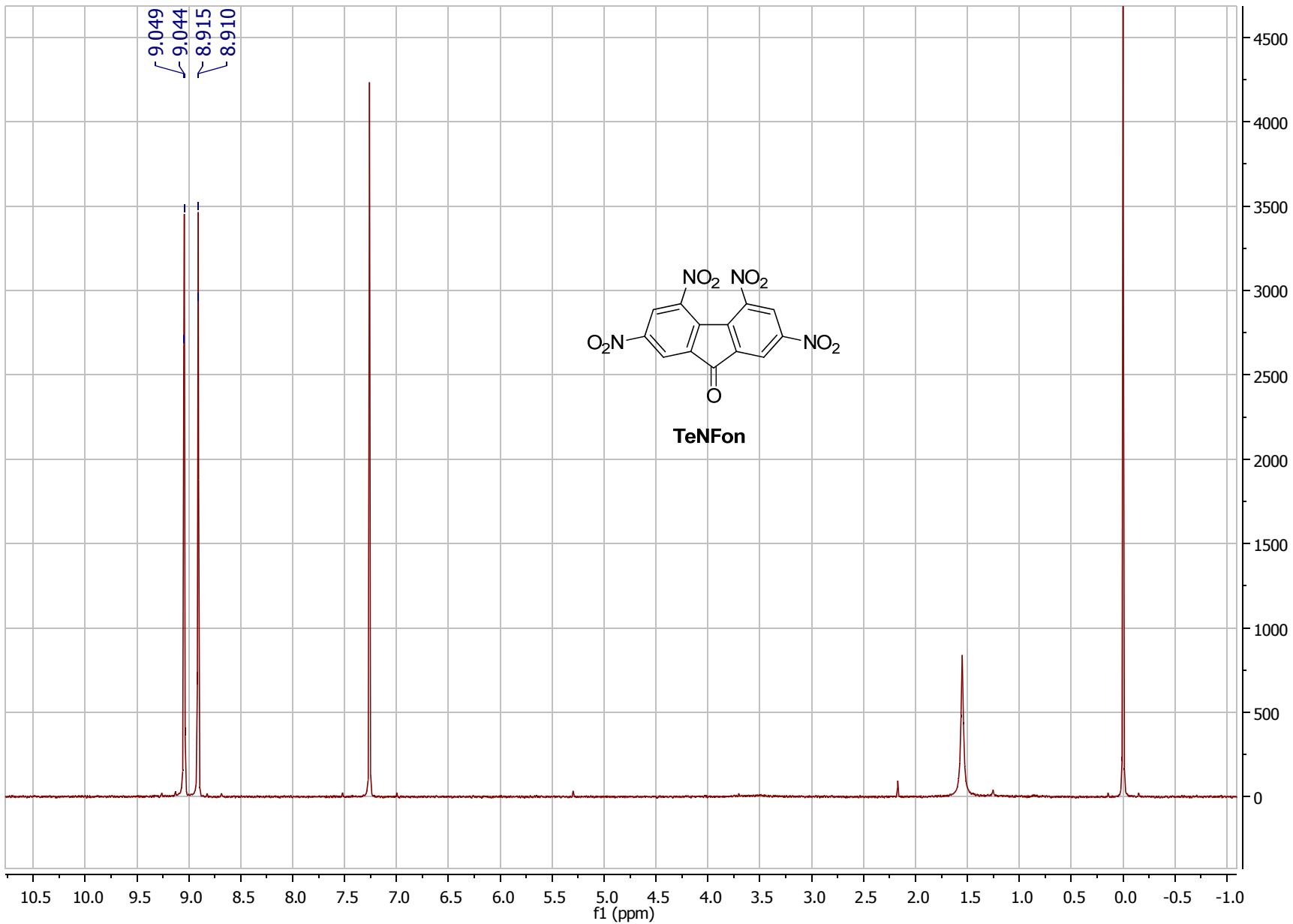


**Figure S9.**  $^1\text{H}$  NMR spectrum of 2,4,5,7-tetranitro-9-fluorenone (**TeN Fon**) in chloroform-*d*.

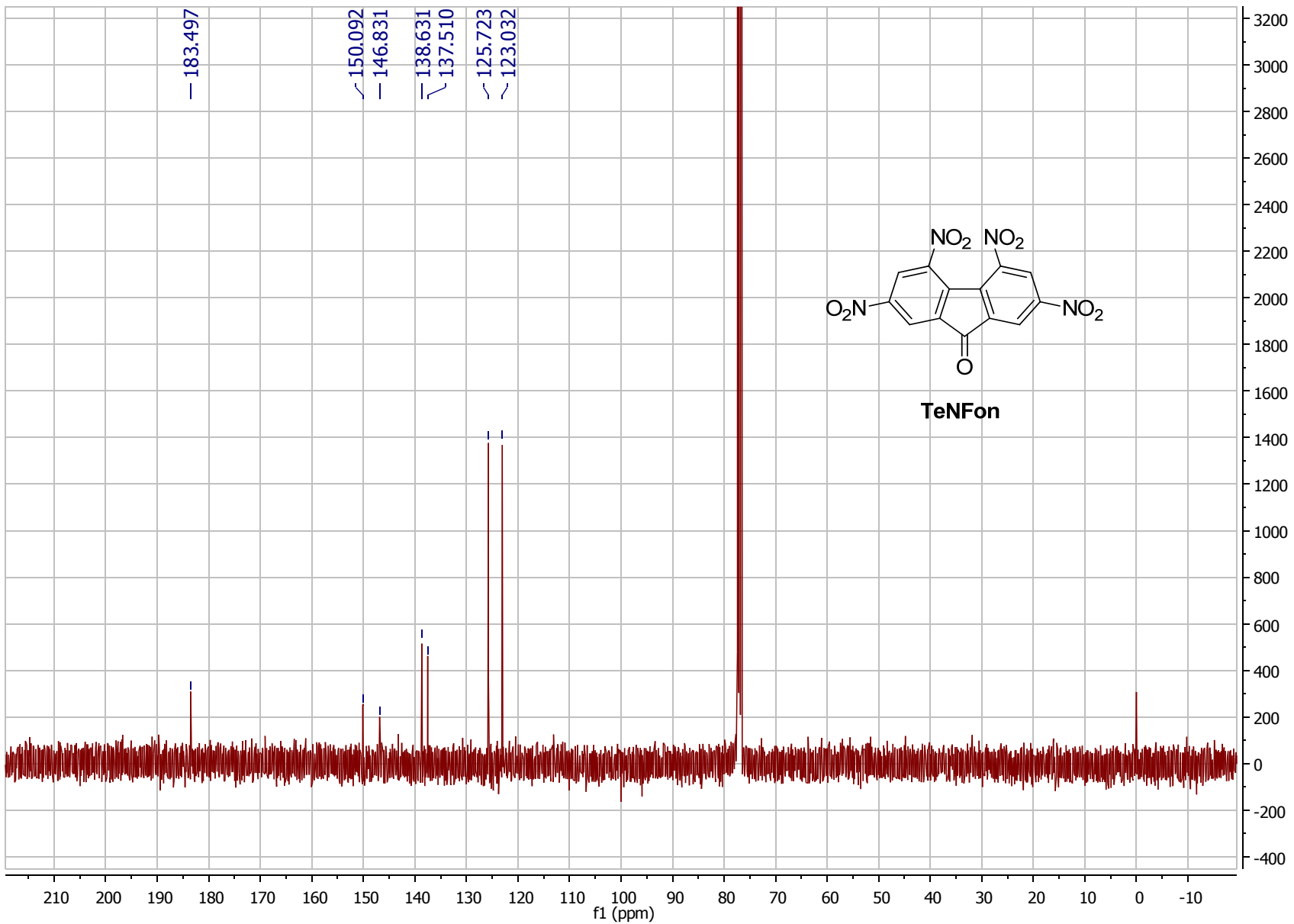


**Figure S10.**  $^{13}\text{C}$  NMR spectrum of 2,4,5,7-tetranitro-9-fluorenone (**TeNFon**) in chloroform- $d$ .

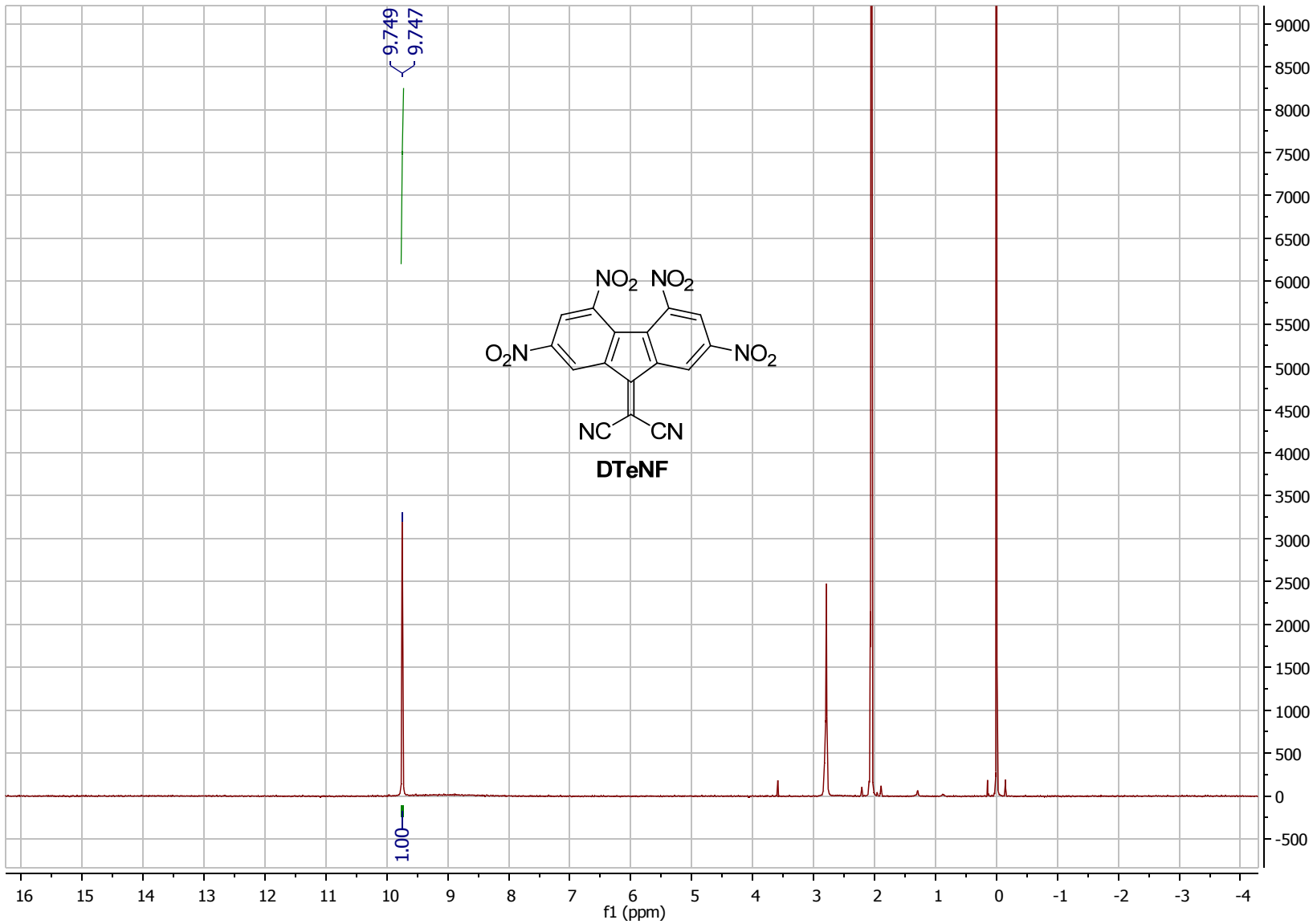


**Figure S11.**  $^1\text{H}$  NMR spectrum of 2,4,5,7-tetranitro-9-dicyanomethylenefluorene (**DTeNF**) in acetone- $d_6$ ; (for  $^1\text{H}$  NMR in acetone- $d_6$ , H-3,6 signals are not observed due to strong paramagnetic broadening, similar to broadening of these signals for other strong fluorene acceptors in polar solvents).<sup>2,3</sup>

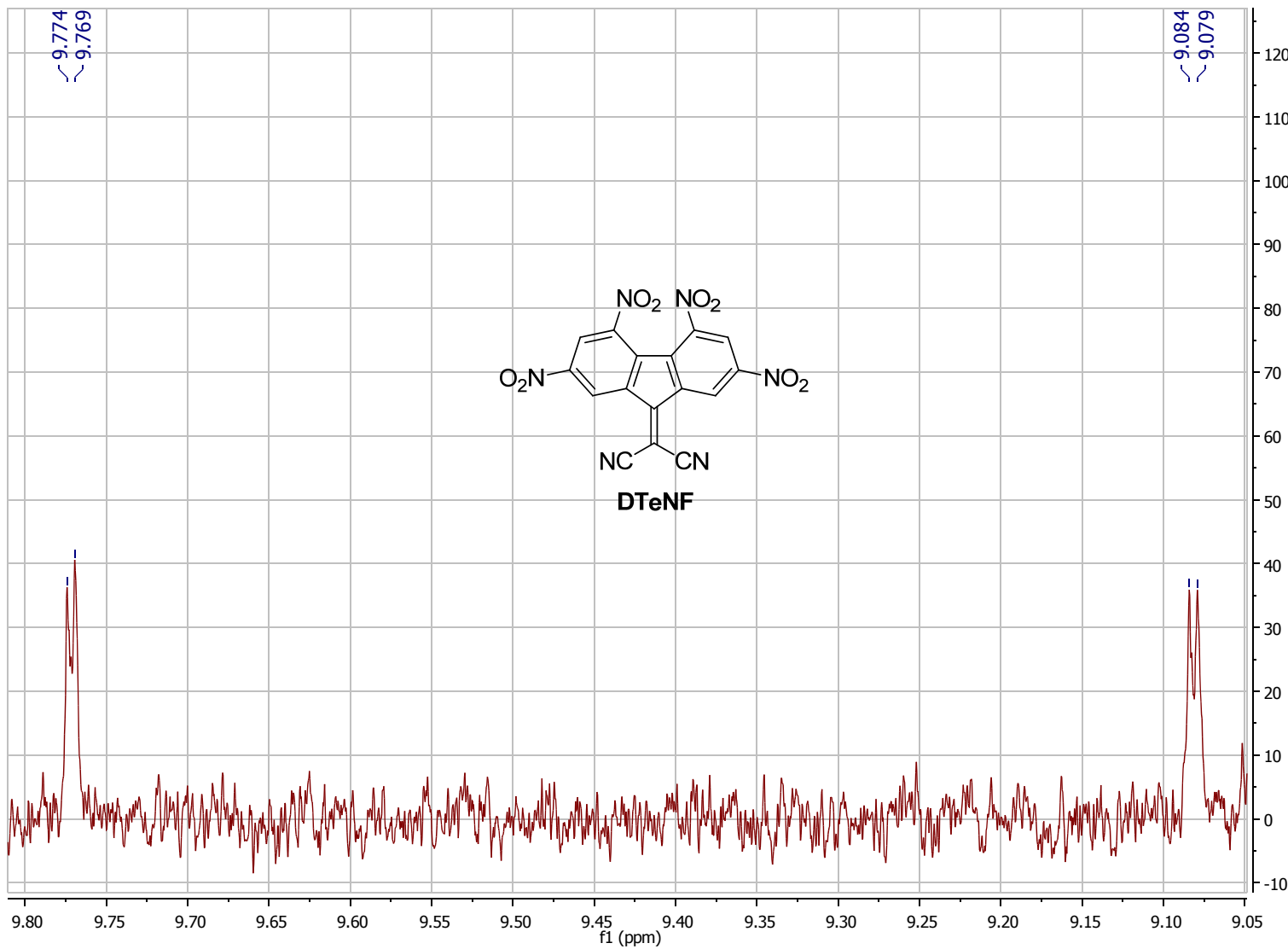


**Figure S12.**  $^1\text{H}$  NMR spectrum of 2,4,5,7-tetranitro-9-dicyanomethylenefluorene (**DTeNF**) in (acetone- $d_6$  + a drop of  $\text{CF}_3\text{COOH}$ ); (for  $^1\text{H}$  NMR in acetone- $d_6$ , H-3,6 signals are not observed due to strong paramagnetic broadening, similar to broadening of these signals for other strong fluorene acceptors in polar solvents; an addition of trifluoroacetic acid recover sharp resonance signals of aromatic protons).<sup>2,3</sup>

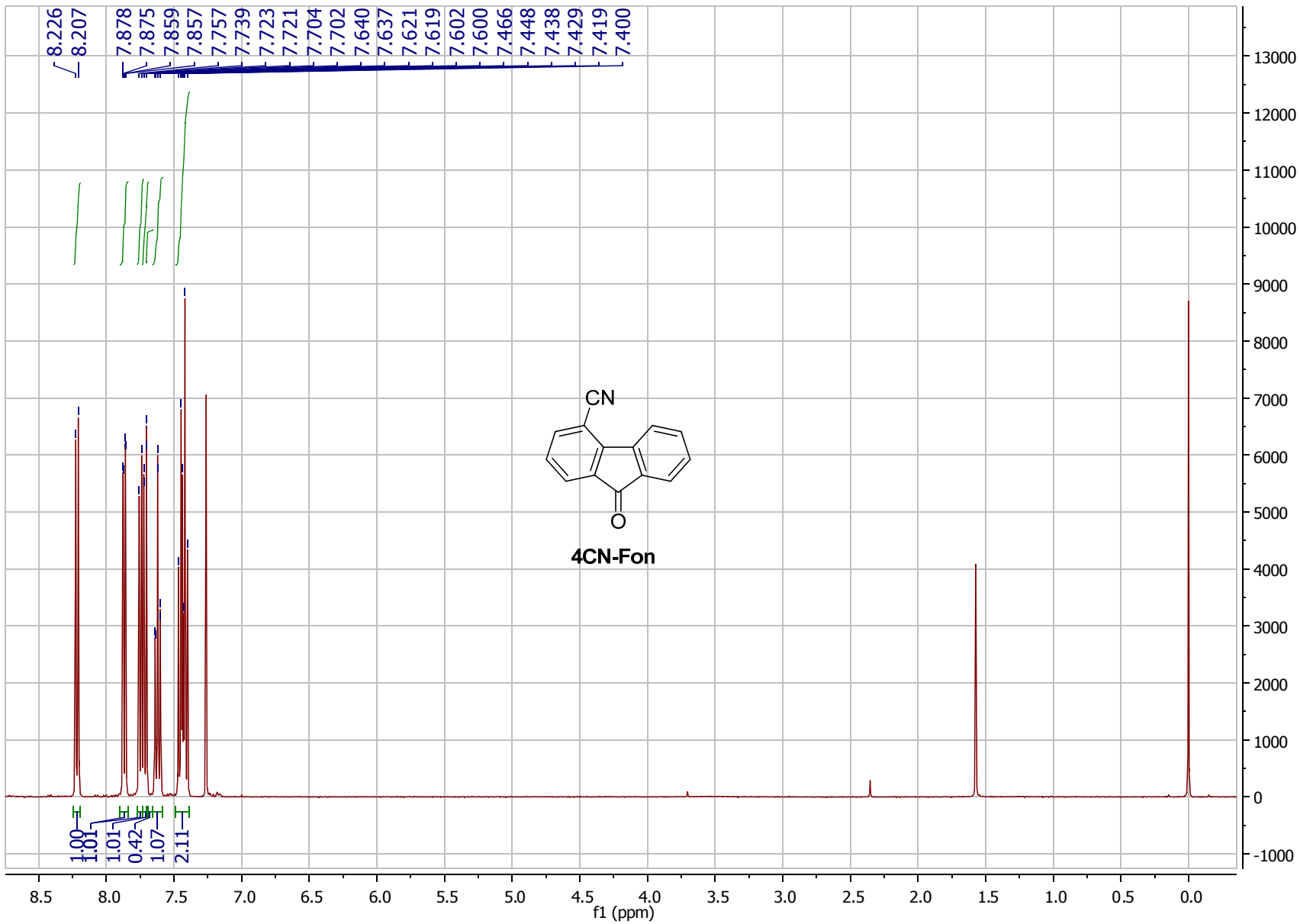


**Figure S13.**  $^1\text{H}$  NMR spectrum of 4-cyano-9-fluorenone (**4CN-Fon**) in chloroform-*d*.

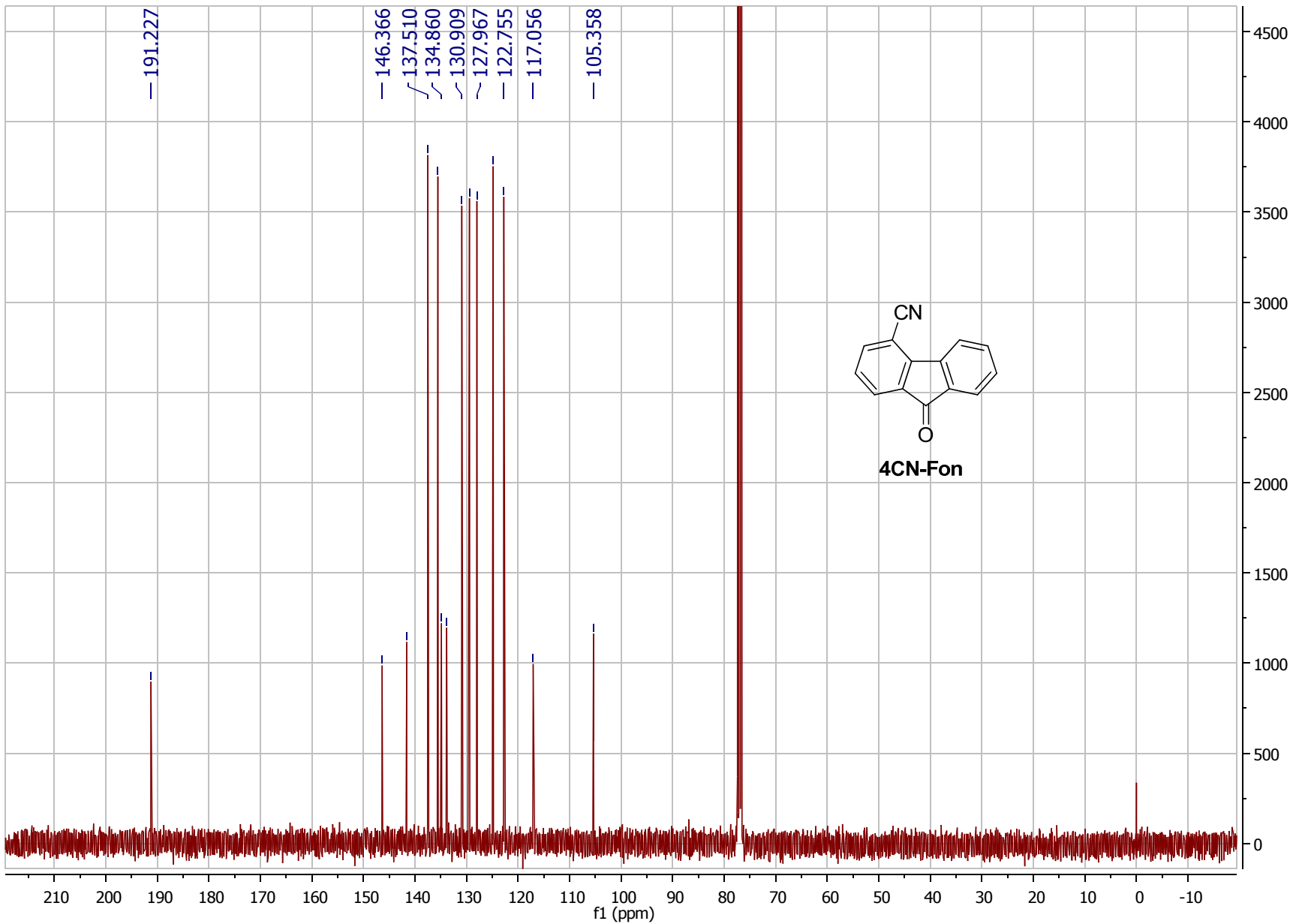


**Figure S14.**  $^{13}\text{C}$  NMR spectrum of 4-cyano-9-fluorenone (**4CN-Fon**) in chloroform-*d*.

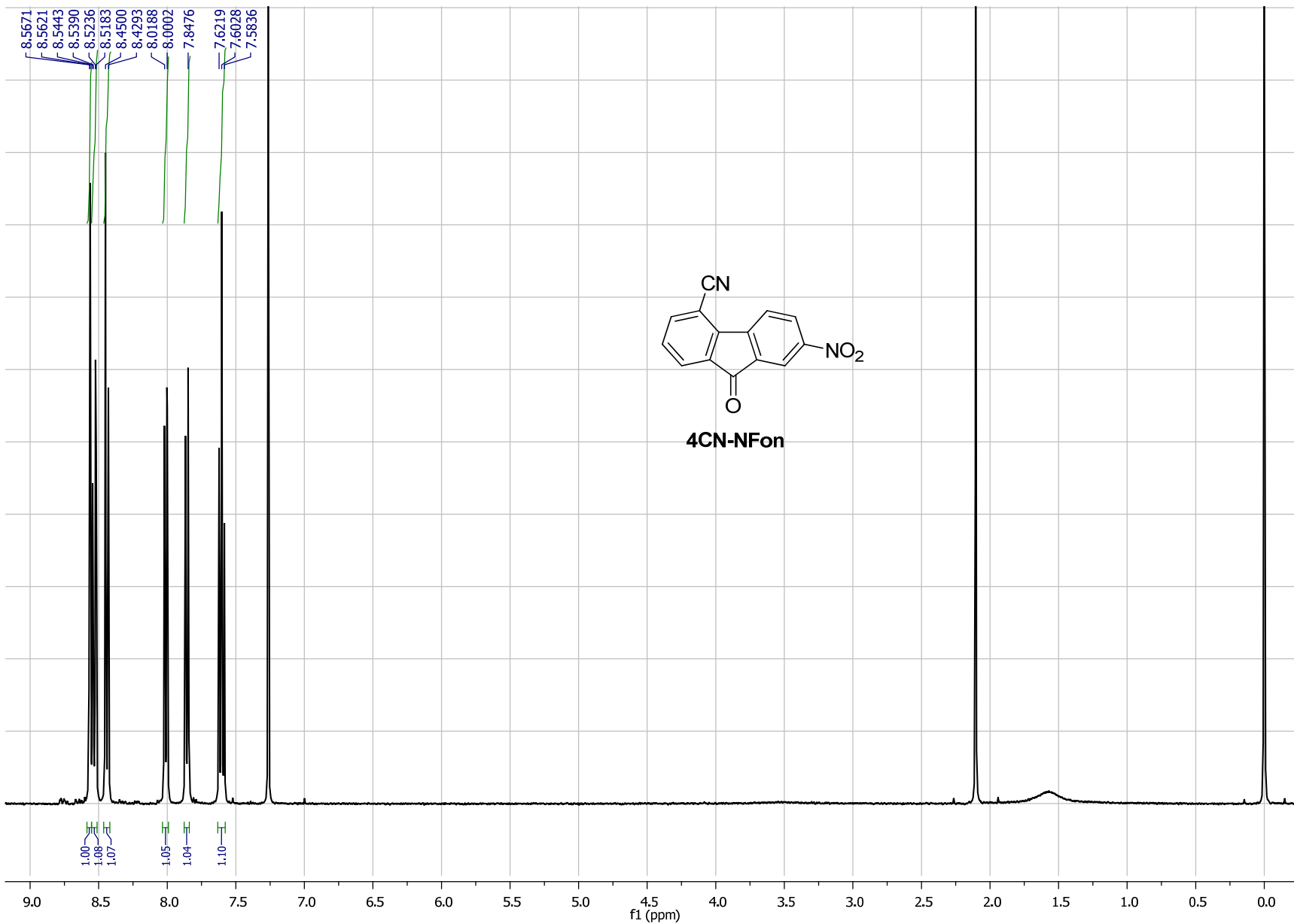


**Figure S15.**  $^1\text{H}$  NMR spectrum of 2-nitro-5-cyano-9-fluorenone (**4CN-NFon**) in chloroform-*d*.

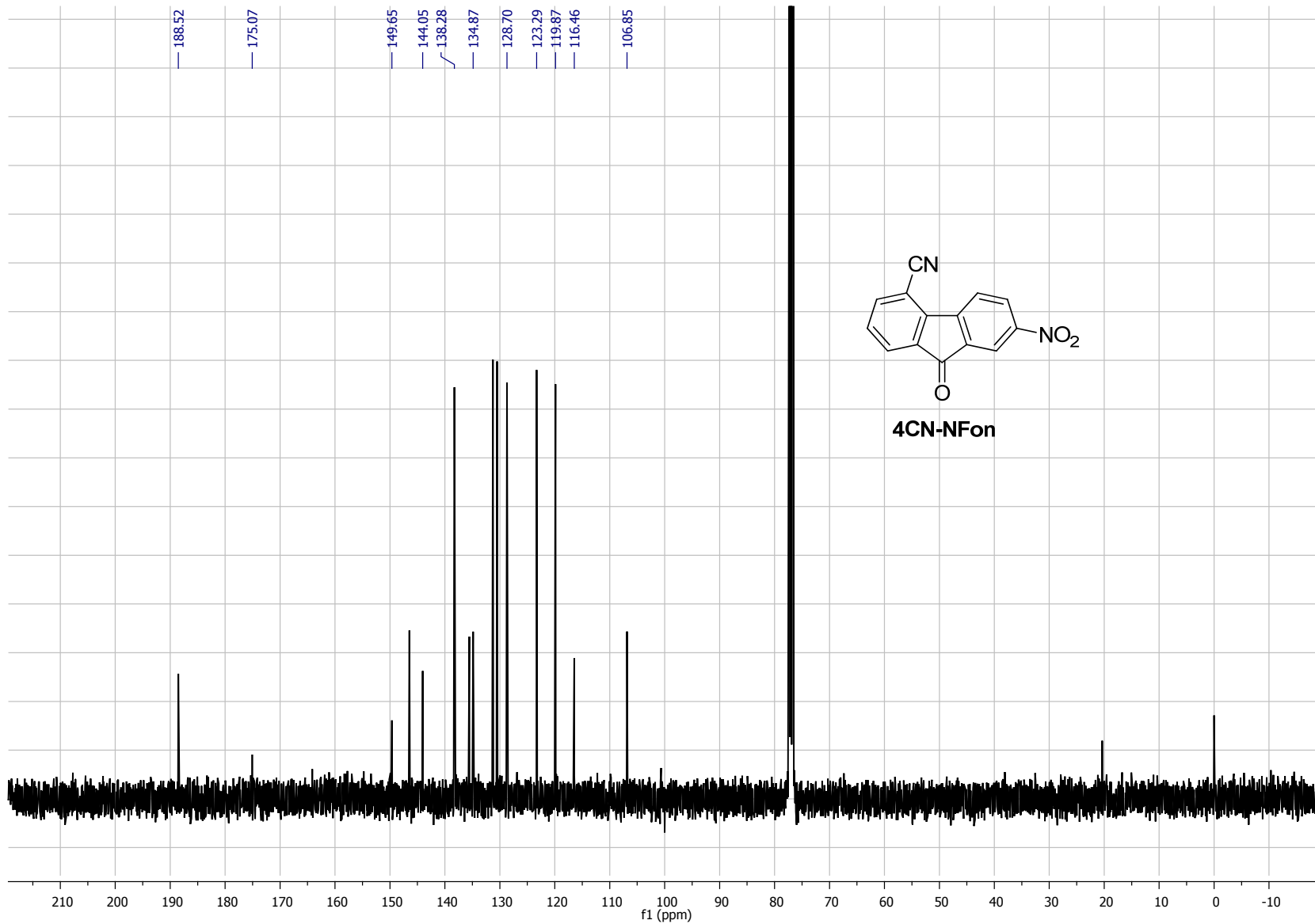


**Figure S16.**  $^{13}\text{C}$  NMR spectrum of 2-nitro-5-cyano-9-fluorenone (**4CN-NFon**) in chloroform-*d*.

### 3. Visible-UV absorption spectra of the acceptors

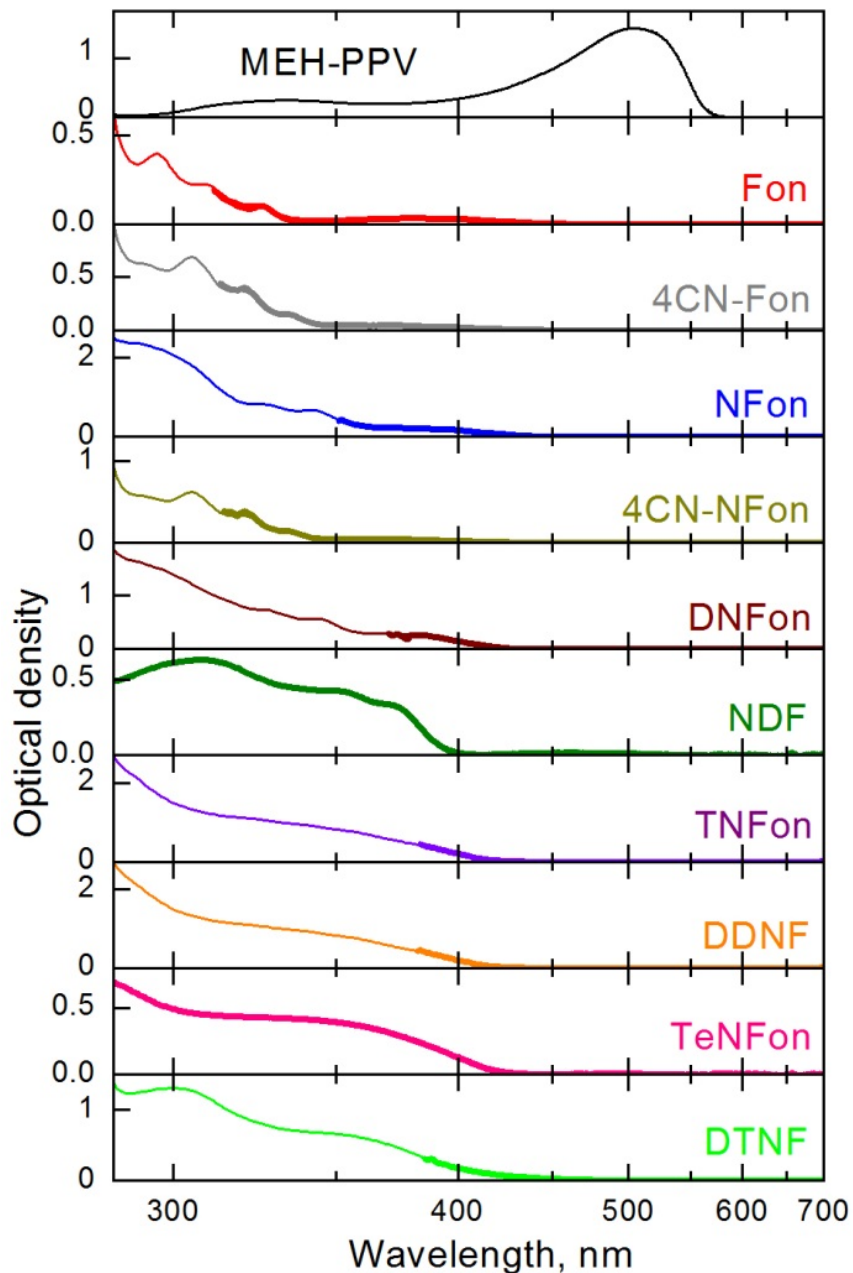


**Figure S17.** UV-Vis absorption spectra of acceptors dissolved in chlorobenzene at concentrations of 2 g/L as used for films preparation (thick lines, rescaled by a factor of ~10) and 0.2 g/L to avoid saturation (thin lines) in a 1 mm path length cuvette. The solvent contribution is subtracted. No signs of aggregation are observed at high acceptor concentration. Absorption spectrum of chlorobenzene solution of MEH-PPV (2 g/L, 0.1 mm path length cuvette) is also given for comparison.

#### **4. DFT B3LYP/6-31+G(d) calculations**

**Table S1.** DFT B3LYP/6-31+G(d) data on total energies of acceptors and derived electron affinities from these calculations (in acetonitrile).

Compound	$E_{total}^{OptN}$ <sup>a</sup> , [hartree]	$E_{total}^{RA\_Opt}$ <sup>b</sup> , [hartree]	$E_{total}^{RA\_F}$ <sup>c</sup> , [hartree]	$EA_V^{DFT}$ <sup>d</sup> , [eV]	$EA_A^{DFT}$ <sup>e</sup> , [eV]
<b>Fon</b>	-575.4664718	-575.5792664	-575.5727114	2.891	3.140
<b>4CN-Fon</b>	-667.7136178	-667.8351259	-667.8282765	3.120	3.379
<b>4CN-NFon</b>	-872.2250702	-872.3658037	-872.3590911	3.647	3.910
<b>NFon</b>	-779.9803134	-780.1144218	-780.1074413	3.459	3.730
<b>DNFon</b>	-984.4912704	-984.6387809	-984.6323670	3.839	4.087
<b>TNFon</b>	-1188.9873311	-1189.1460557	-1189.1395367	4.142	4.393
<b>TeNFon</b>	-1393.4784054	-1393.6494801	-1393.6429800	4.478	4.725
<b>NDF</b>	-928.5397925	-928.6875699	-928.6827937	3.891	4.081
<b>DDNF</b>	-1133.0496864	-1133.2076768	-1133.2027609	4.165	4.356
<b>DTNF</b>	-1337.5436888	-1337.7112890	-1337.7061082	4.420	4.621
<b>DTeNF</b>	-1542.0335240	-1542.2121200	-1542.2065954	4.710	4.869

<sup>a</sup>  $E_{total}^{OptN}$  is a total energy for the optimized geometry of the neutral state of the acceptor.

<sup>b</sup>  $E_{total}^{RA\_Opt}$  is a total energy for the optimized geometry of radical anion state of the acceptor.

<sup>c</sup>  $E_{total}^{RA\_F}$  is a total energy for single point calculation of radical anion state at frozen optimized geometry of the neutral state.

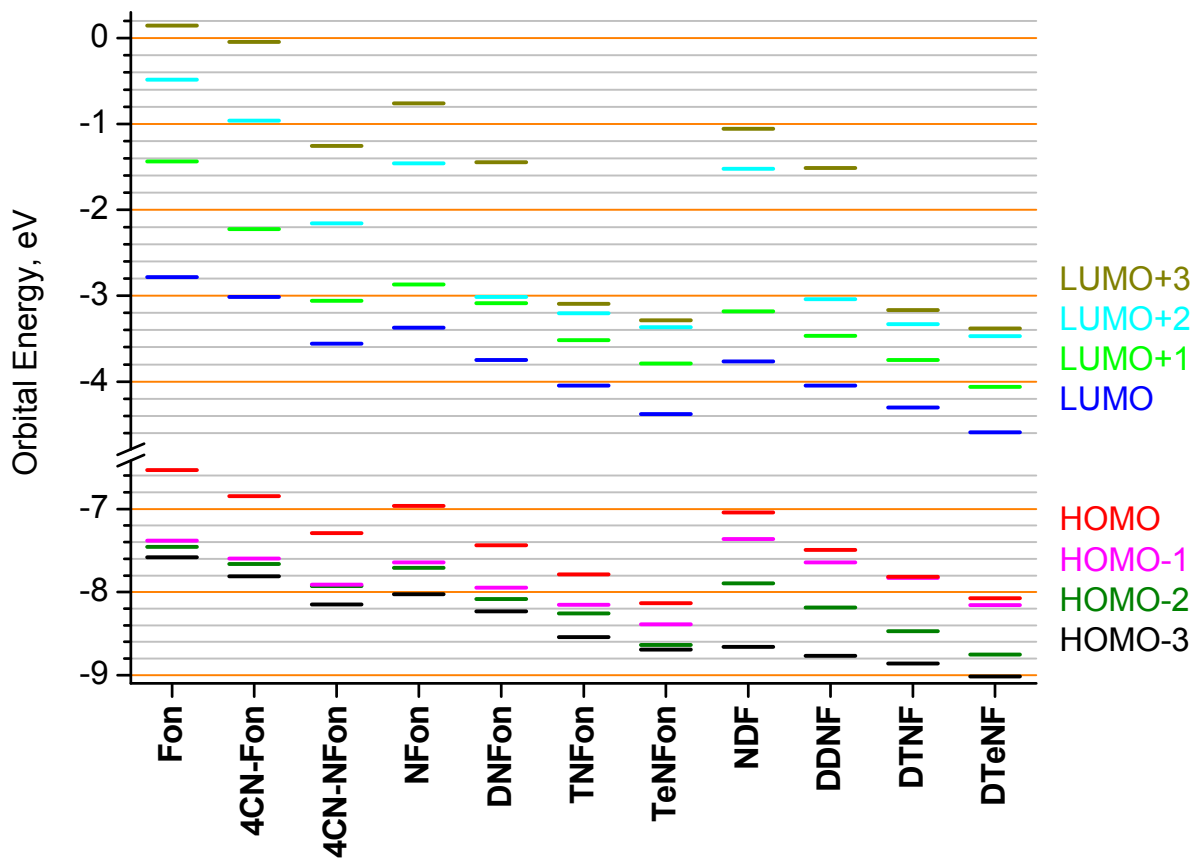
<sup>d</sup>  $EA_V^{DFT}$  is calculated vertical electron affinity of the acceptor, according to equation:

$$EA_V^{DFT} = E_{total}^{OptN} - E_{total}^{RA\_F}.$$

<sup>e</sup>  $EA_A^{DFT}$  is calculated adiabatic electron affinity of the acceptor (including zero point energy corrections), according to equation:

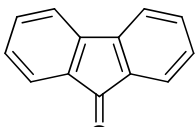
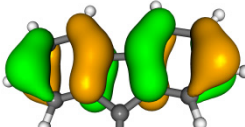
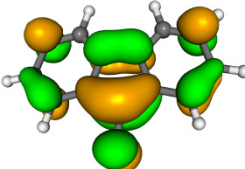
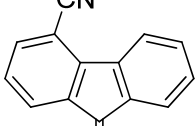
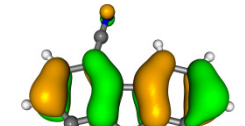
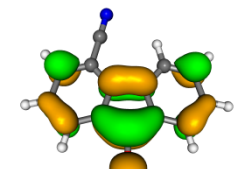
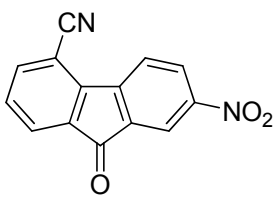
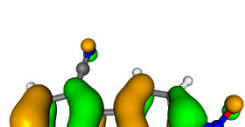
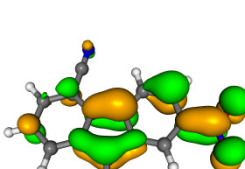
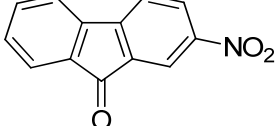
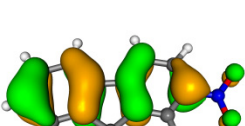
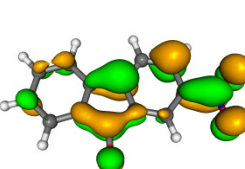
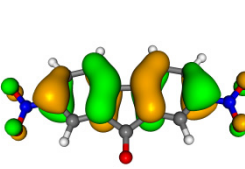
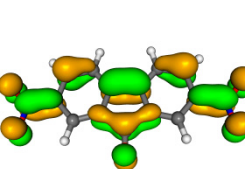
$$EA_A^{DFT} = E_{total}^{OptN} - E_{total}^{RA\_Opt} + ZPE^N - ZPE^{RA},$$

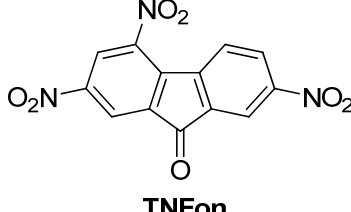
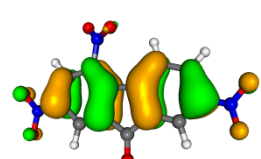
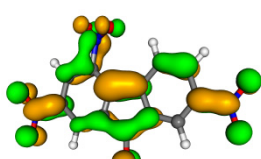
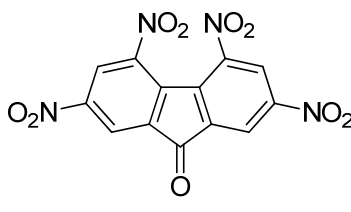
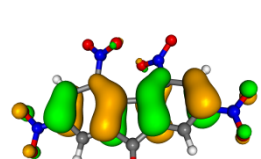
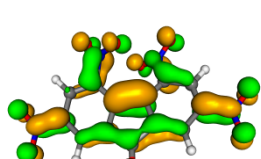
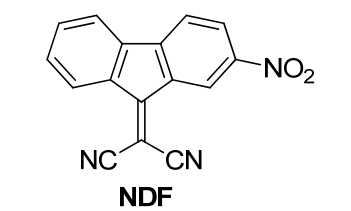
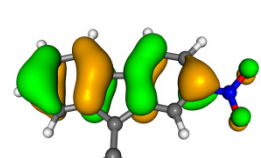
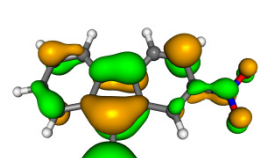
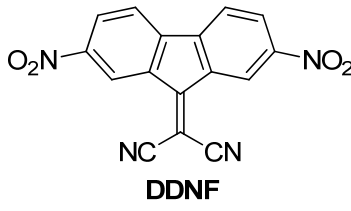
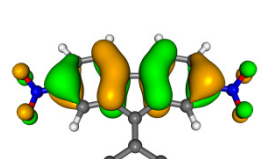
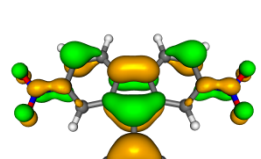
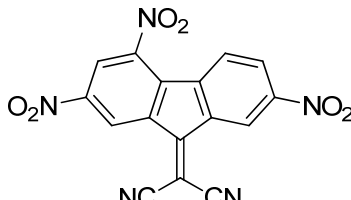
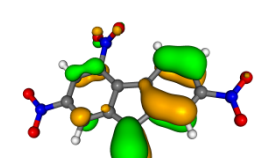
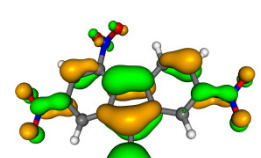
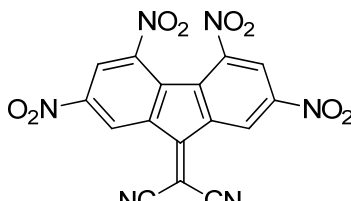
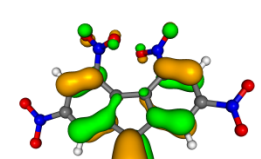
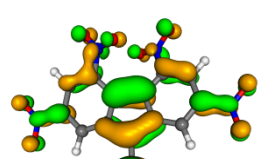
where  $ZPE^N$  and  $ZPE^{RA}$  are zero point energies for optimized geometries of neutral and radical anion state, respectively.



**Figure S18.** Orbital energy diagram of fluorene electron acceptors from B3LYP/6-31+G(d) calculations in acetonitrile.

**Table S2.** HOMO and LUMO orbital coefficients of fluorene acceptors from B3LYP/6-31+G(d) calculations in acetonitrile.

Compound	HOMO, eV	LUMO, eV
 <b>Fon</b>	 -6.534	 -2.781
 <b>4CN-Fon</b>	 -6.847	 -3.013
 <b>4CN-NFon</b>	 -7.292	 -3.555
 <b>NFon</b>	 -6.966	 -3.372
 <b>DNFon</b>	 -7.435	 -3.749

 <b>TNFon</b>		
	<b>-7.789</b>	<b>-4.045</b>
 <b>TeNFon</b>		
	<b>-8.136</b>	<b>-4.377</b>
 <b>NDF</b>		
	<b>-7.041</b>	<b>-3.768</b>
 <b>DDNF</b>		
	<b>-7.492</b>	<b>-4.045</b>
 <b>DTNF</b>		
	<b>-7.815</b>	<b>-4.302</b>
 <b>DTeNF</b>		
	<b>-8.074</b>	<b>-4.591</b>

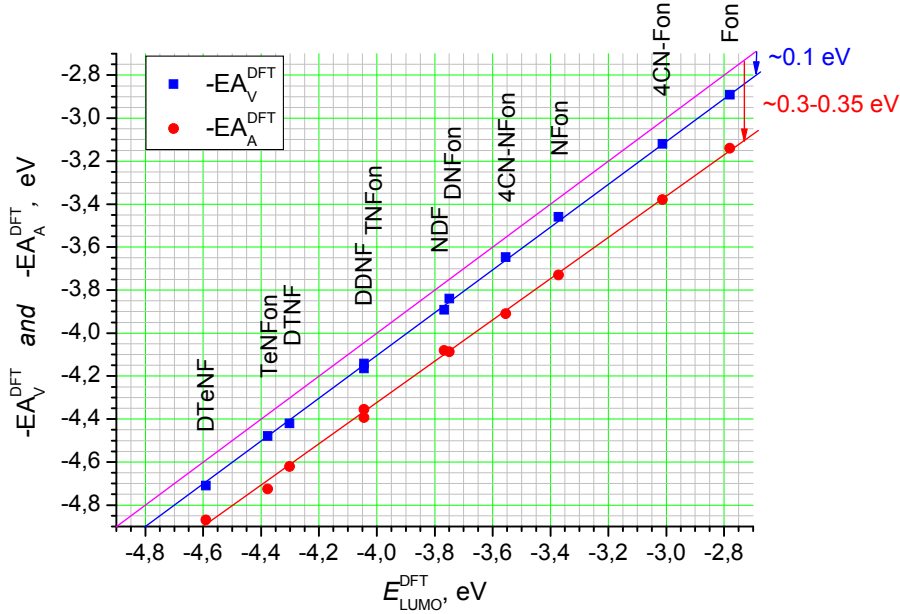


**Figure S19.** Correlations between LUMO energies and vertical and adiabatic electron affinities for studied fluorene acceptors (DFT B3LYP/6-31+G(d) in acetonitrile). Solid blue and red lines are linear fits of the data, solid magenta line corresponds to the bisection of the equal energies. Calculated  $\text{EA}_V^{\text{DFT}}$  and  $\text{EA}_A^{\text{DFT}}$  are lower than calculated  $E_{\text{LUMO}}^{\text{DFT}}$  energies by  $\sim 0.1$  eV and  $\sim 0.3\text{--}0.35$  eV, respectively.

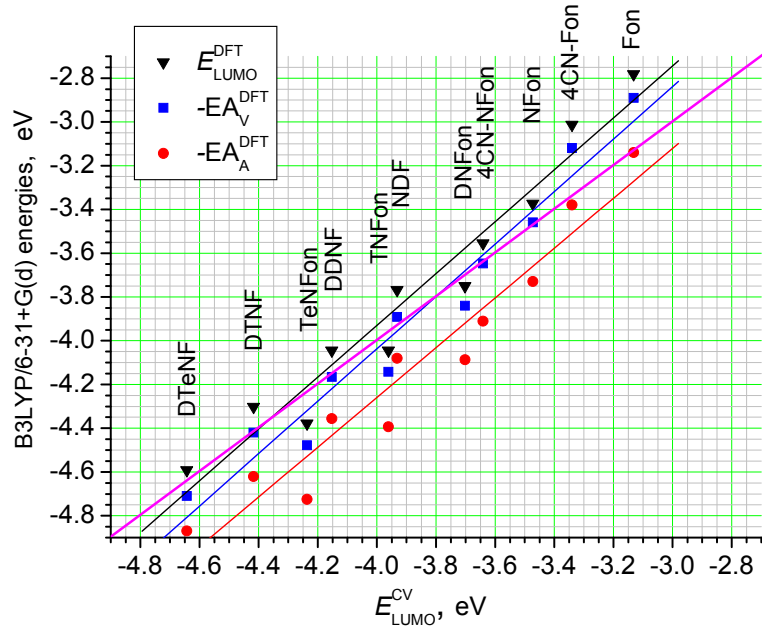


**Figure S20.** Correlations of B3LYP/6-31+G(d) calculated  $E_{\text{LUMO}}^{\text{DFT}}$  orbital energies, vertical and adiabatic electron affinities,  $\text{EA}_V^{\text{DFT}}$  and  $\text{EA}_A^{\text{DFT}}$ , versus experimental  $E_{\text{LUMO}}^{\text{CV}}$  values from cyclic voltammetry measurements (all are in acetonitrile). Solid black, blue and red lines are linear fits of the data, solid magenta line corresponds to the bisection of the equal energies.

## **5. Ultrafast spectroscopy data**

**Table S3.** The fitting parameters of pristine MEH-PPV and MEH-PPV:acceptors transients . The weight coefficients of the respective times (Eq.1) are given in parentheses. Excitation wavelength is 560 nm.

Compound	Isotropic decay			Averaged recombination time $\langle \tau \rangle$
	$\tau_1 (A_1)$	$\tau_2 (A_2)$	$A_0$	
MEH-PPV	50 ps (0.65)	3 ps (0.25)	0.12	49.3 ps
<b>Fon</b>	55 ps (0.65)	3 ps (0.2)	0.15	54.7 ps
<b>4CN-Fon</b>	47 ps (0.78)	-	0.22	47 ps
<b>NFon</b>	37 ps (0.8)	2.5 ps (0.2)	-	36.4 ps
<b>4CN-NFon</b>	21 ps (1)	-	-	21 ps
<b>DNFon</b>	20 ps (0.82)	1 ps (0.18)	-	19.8 ps
<b>NDF</b>	12 ps (1)	-	-	12 ps
<b>TNFon</b>	7 ps (1)	-	-	7 ps
<b>DDNF</b>	2.7 ps (0.6)	0.7 ps (0.35)	0.05	2.4 ps
<b>TeNFon</b>	1.7 ps (0.98)	65 ps (0.02)	-	1.7 ps
<b>DTNF</b>	1 ps (0.8)	-	0.03	1 ps

To analyze the isotropic signal we have used the following bi-exponential fitting function:

$$\Delta T_{ISO} = A_0 + A_1 \exp\left(-\frac{t}{\tau_1}\right) + A_2 \exp\left(-\frac{t}{\tau_2}\right) \quad (1)$$

where  $A_i$  and  $\tau_i$  are the amplitudes and the time constants, respectively, and the sum of all amplitudes is normalized to 1. The averaged recombination time was calculated as a weighed mean of the two recombination times in Eq.1:

$$\langle \tau \rangle = \frac{A_1 \tau_1^2 + A_2 \tau_2^2}{A_1 \tau_1 + A_2 \tau_2} \quad (2)$$

## REFERENCES

- (1) Zhang, X.; Han, J. B.; Li, P. F.; Ji, X.; Zhang, Z. Improved, Highly Efficient, and Green Synthesis of Bromofluorenones and Nitrofluorenones in Water. *Synth. Commun.* **2009**, *39*, 3804–3815.
- (2) Mysyk, D. D.; Perepichka, I. F.; Sokolov, N. I. Electron Acceptors of the Fluorene Series. 6. Synthesis of 4,5-Dinitro-9-X-fluorene-2,7-disulfonic Acid Derivatives, Their Charge Transfer Complexes with Anthracene and Sensitization of Photoconductivity of Poly-*N*-(2,3-epoxypropyl)carbazole. *J. Chem. Soc., Perkin Trans. 2* **1997**, 537–545.
- (3) Perepichka, I. F.; Kuz'mina, L. G.; Perepichka, D. F.; Bryce, M. R.; Goldenberg, L. M.; Popov, A. F.; Howard, J. A. K., Electron Acceptors of the Fluorene Series. 7. 2,7-Dicyano-4,5-dinitro-9-X-fluorenes: Synthesis, Cyclic Voltammetry, Charge Transfer Complexation with N-Propylcarbazole in Solution, and X-Ray Crystal Structures of Two Tetrathiafulvalene Complexes. *J. Org. Chem.* **1998**, *63*, 6484–6493.
- (4) Mukherje, T. K. Photoconductivity of Electron Acceptors. I. Nitro Derivatives of Fluoren- $\Delta^{9a}$ -malononitrile. *J. Phys. Chem.* **1966**, *70*, 3848–3852.
- (5) Perepichka, D. F.; Perepichka, I. F.; Ivasenko, O.; Moore, A. J.; Bryce, M. R.; Kuz'mina, L. G.; Batsanov, A. S.; Sokolov, N. I. Combining High Electron Affinity and Intramolecular Charge Transfer in 1,3-Dithiole–Nitrofluorene Push-Pull Diads. *Chem.–Eur. J.* **2008**, *14*, 2757–2770.
- (6) Orchin, M.; Reggel, L.; Woolfolk, E. O. Molecular Complexes with 2,4,7-Trinitrofluorenone. II. *J. Am. Chem. Soc.* **1947**, *69*, 1225–1227.
- (7) Orchin, M.; Woolfolk, E. O. Molecular Complexes with 2,4,7-Trinitrofluorenone. *J. Am. Chem. Soc.* **1946**, *68*, 1727–1729.
- (8) Perepichka, D. F.; Bryce, M. R.; Perepichka, I. F.; Lyubchik, S. B.; Christensen, C. A.; Godbert, N.; Batsanov, A. S.; Levillain, E.; McInnes, E. J. L.; Zhao, J. P. A ( $\pi$ -Extended Tetrathiafulvalene)–Fluorene Conjugate. Unusual Electrochemistry and Charge Transfer Properties: The First Observation of a Covalent  $D^{2+}–\sigma–A^{\bullet-}$  Redox State. *J. Am. Chem. Soc.* **2002**, *124*, 14227–14238.
- (9) Perepichka, I. F.; Popov, A. F.; Orekhova, T. V.; Bryce, M. R.; Andrievskii, A. M.; Batsanov, A. S.; Howard, J. A. K.; Sokolov, N. I. Electron Acceptors of the Fluorene Series. 10. Novel Acceptors Containing Butylsulfanyl, Butylsulfinyl, and Butylsulfonyl Substituents: Synthesis, Cyclic Voltammetry, Charge-Transfer Complexation with Anthracene in Solution, and X-Ray Crystal Structures of Two Tetrathiafulvalene Complexes. *J. Org. Chem.* **2000**, *65*, 3053–3063.
- (10) Perepichka, I. F.; Popov, A. F.; Orekhova, T. V.; Bryce, M. R.; Vdovichenko, A. N.; Batsanov, A. S.; Goldenberg, L. M.; Howard, J. A. K.; Sokolov, N. I.; Megson, J. L. Electron Acceptors of the Fluorene Series. 5. Intramolecular Charge Transfer in Nitro-sbstituted 9-(Aminomethylene)fluorenes. *J. Chem. Soc., Perkin Trans. 2* **1996**, 2453–2469.
- (11) Mukherje, T. K.; Levasseur L. A. 9-Dicyanomethylene-2,4,7-trinitrofluorene, a New Electron Acceptor. *J. Org. Chem.* **1965**, *30*, 644–646.
- (12) Ray, F. E.; Francis, W. C. Polynitrocompounds of Fluorene. *J. Org. Chem.* **1943**, *8*, 52–59.
- (13) Huntress, E. H.; Pfister 3rd., K.; Pfister, K. H. T. Fluorenones and Diphenic Acids. IX. Establishment of Authentic 1-Bromo- and 4-Bromofluorenones. *J. Am. Chem. Soc.* **1942**, *64*, 2845–2849.
- (14) Liu, B. J.; Hu, W.; Robertson, G. P.; Guiver, M. D. Poly(aryl ether ketone)s with Carboxylic Acid Groups: Synthesis, Sulfonation and Crosslinking. *J. Mater. Chem.* **2008**, *18*, 4675–4682.
- (15) Mysyk, D. D.; Perepichka, I. F.; Sivchenkova, N. M.; Kostenko, L. I.; Pototskii, I. S; Baratvov, A. G. Substituted 4-Cyanofluorenes as Sensitizers of Photoconductivity of Polymers Based on Carbazolyl Substituted Monomers. USSR Patent No 1,092,151 (15.01.1984); *Bulletin of Invents*, **1984**, No 18 (in Russian).
- (16) Mysyk, D. D.; Perepichka, I. F.; Sivchenkova, N. M.; Kampars, V. E.; Neilands, O. Ya.; Kampare, R. B. Electron Acceptors of the Fluorene Series. I. Syntheses and Electron Affinities of Substituted 4-Cyanofluorenes. *Izvestiya Akad. Nauk Latvijskoj SSR, Ser. Khim. (Latvijas PSR Zinātņu Akademijas Vēstis, Ķīmijas sērija)* **1984**, 328–331 (in Russian).
- (17) Stankevičius, I. P.; Janušiene, L. N.; Terent'ev, P. B.; Saprogoniene, M. S. A Procedure for Preparing 4-Cyanofluoren-9-one. *Russ. J. Appl. Chem.* **2006**, *79*, 1384–1385 (in Russian).
- (18) Mysyk, D. D.; Perepichka, I. F.; Edgina, A. S.; Neilands, O. Ya. Electron Acceptors of Fluorene Series. IV. Synthesis of Nitrosubstituted 4-Cyanofluorenes and Evaluation of Their Electron Affinity Using Redox Potential Values. *Latvian J. Chem.* **1991**, 727–735 (in Russian).